Nicolas Viltard
LATMOS
CNRS-UVSQ-UPMC
11 Blvd d'Alembert
Quartier des Garennes
78280 Guyancourt France
tel: +33 1 80 28 52 33
email: nicolas.viltard@latmos.ipsl.fr

Visiting scientist's report

August 2012-January 2013

DSA/CPTEC/INPE

Funded by FAPESP n° 2012/11441-5

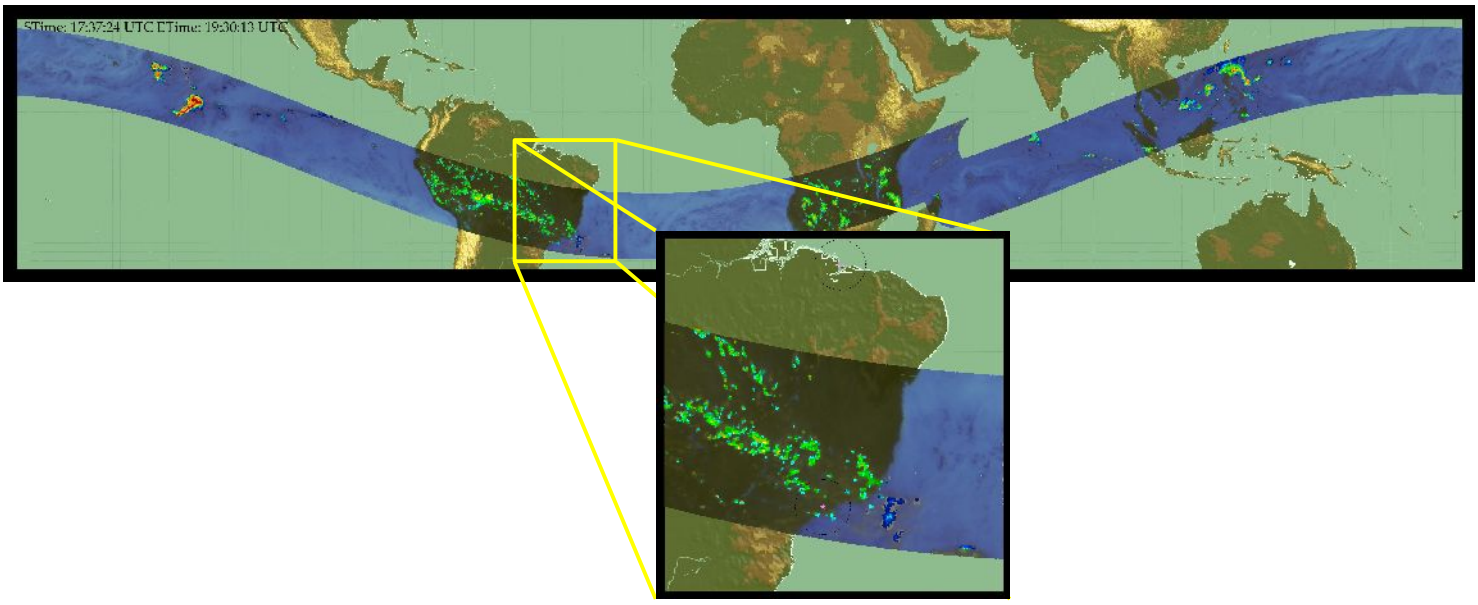

MADRAS at 17h40 over CHUVA VAP field experiment while afternoon convection develops.

1. Context and foreseen work

(Note: the WP 1 to 4 in the chapters 3 to 5 refer to the work packages of the initial proposal)

The project of my 6-month visit at INPE/Divisaõ de Systemais Ambientes regards the properties of the rain regimes over Brasil and the retrieval of instantaneous rain itself from passive microwave radiometers on board low-orbiting satellites. Brazil is partially covered with raingages and radar networks but it is easily understandable that satellite-based rain estimations could provide a homogeneous retrieval of the rain over the whole country while the satellite data are easily accessible. Nevertheless, as explained hereafter, satellite based rain estimates are strongly dependent on a number of rain-related parameters that can affect the algorithms performances.

This research effort is also conducted in the framework of the CHUVA campaign which is aimed at deploying a series of instruments in various locations over Brazil in order precisely to better characterize the various rain regimes. Among those instruments, the most useful for our purpose here, is the X-Band dual polarization Doppler radar because it can give a good assessment of the rain amount that falls on the ground and help validate the satellite product, but also it allows us to get information about the "local" microphysics of the precipitation.

The knowledge of the properties of the precipitations is a very important information in order to retrieve accurately the rain from a vector of microwave brightness temperatures (Tb). Over land in particular, the surface emissivity offers for all frequencies below ~40 GHz a very strong signal which will mask most of the rain/precipitation contribution: at these frequencies the rain is mostly characterized by emission by the liquid drops. If the background is already warm, there is no contrast between rain and/no-rain.

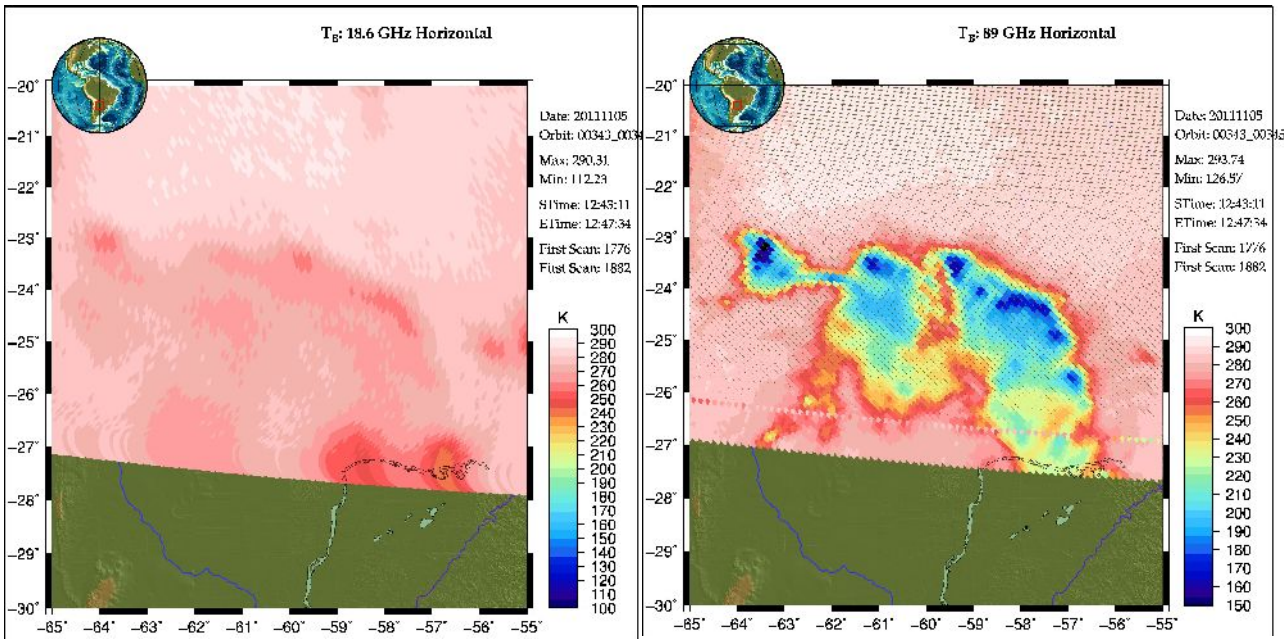

Figure 1.1*: Megha-Tropiques MADRAS brightness temperatures at 18.6 GHz (left) and 89 GHz (right) of a Mesoscale convective system. The 19 GHz is showing a slight signal which is likely due to the surface emissivity change by the rain while the 89 GHz shows a strong signature of ice scattering. On the latter image, the convective regions are characterized by heavier scattering with Tbs below 160-170 K (deep blue) while the stratiform region is characterized by Tbs between 170 and 230 K (light blue to yellow) and the more "anvil" region by Tbs between 230 and 260 K (orange and deep red). The Tbs warmer than that (light red to pinkish) are most likely the non-precipitating regions or regions where no ice is present in the upper part of the cloud.*

From **Figure 1.1** it can be seen that over land, the rain retrieval has to be performed mostly from the information available in the higher frequency channels (above 35 GHz) and from the ice scattering. This has a direct consequence on our ability to detect early stages of convection and warm rain situations which will not have a developed ice phase. It can be seen on the 19 GHz image that there is somewhat slight variation of the brightness temperature were the 89 GHz tells us that is is likely raining. Unfortunately, the natural variability of the surface emissivity will provide a much larger signal on the brightness temperature over land at the lower frequency than the rain itself. The correlation between the two images and the precipitation presence is artificially enhanced by our a-priori knowledge deduced from the 89 GHz information.

The classical mental scheme of tropical convection is well documented through literature (see Houze (1993), "Cloud Dynamics" for instance). In an unstable environment convection is triggered by a disturbance of whatever nature. A cloud forms an develops vertically depending on the local or regional conditions. Whenever super saturated air parcels are lifted above the freezing level, cold processes will take place and ice particles will start to form. These particles will grow according to a number of microphysical processes which are beyond the scope of the present report, but their fall speed will be balanced by the vertical motion of air due to the convective activity. At some point, the particles fall speed will be larger than the vertical motion of air and the particles will fall. The more intense the vertical motion, the larger the particles can be before falling. The lighter particles will tend to be advected vertically and horizontally outside of the convective region. These particles will progressively build the stratiform region associated to the convective cell. As convection develops, the stratiform part develops equally. When the convection stops, the stratiform part, mostly built of lighter particles will remain longer until most of the precipitating ice has either fallen or evaporated. At the end only remains the cloud ice particles that will constitute the remaining anvil cirruses. This oversimplified vision of the convection life-cycle is meant to illustrate the connection between the later and the microphysics properties of the ice crystals. In the convective region, the rain falling on the ground will be a mix of the warm processes (condensation of liquid rain) and the cold processes (melting of dense/heavy ice crystals). In the stratiform, most rain will come from falling and melting ice crystals.

From this conceptual model, one can immediately see that the rain that will be retrieved over land from the scattering signature at 37, 89 and eventually 150 GHz channels of Passive Microwave Radiometers (PMR) will be strongly dependent on the ice properties which in turns is very dependent of the life cycle of the observed convection.

The life cycle of convection cannot really be observed by PMR since those sensors are only found on low-orbiting satellites that will overpass a rain system at best twice a day (with the notable exception of MADRAS on Megha-Tropiques). The only instrument really suitable to characterize the life cycle of convection are indeed the infrared imagers on the geostationary satellite that will take an image every 15 or 30'. This was the main motivation of my visit to DSA/CPTEC/INPE, where an internationally recognized expertise has been developed over the years in using IR techniques to characterize the life cycle of convection over Brazil and South America. Furthermore, the series of CHUVA campaigns give an excellent testbed for validation of the satellite products and the microphysics characterization of ice using the polarimetric X-band radar mentioned above.

From what is said above, the following work plan was envisioned: from the ForTraCC (Vila et al 2008) IR-based tracking method, build a database of system which were overpassed by the TRMM satellite. The ForTraCC will provide us with the life stage of the system at the moment of the overpass while the TMI brightness temperature are collected. The brightness temperatures and

surface precipitation relationship remains the same regardless of the life cycle but eventually its application differs for each life stage. The underlying idea being that, for instance, a lot of snow from a large stratiform part (typically a dissipating stage) and a few graupel (from a small convective cell at its initiation stage) can provide the same amount of scattering, but still have very different rain intensities at the ground. The retrieval algorithm cannot distinguish between these two situation without some external information.

Once this life cycle is implemented in the retrieval algorithm, it would be possible to assess the impact of the implementation and validate it using CHUVA data. Then see if we can use this technique of PMR+IR to retrieve the warm rain situation when no signature is visible in the scattering channels and some weak signal can be eventually found in the emission channels. In such case, the life cycle information could provide us with the information that rain might be present and a retrieval could be attempted for the given pixel. The error bar would be large but some undetected rain could hopefully be retrieved.

2. Principle of the rain retrieval algorithm BRAIN

In order to understand a number of aspects of the present report, it is necessary to explain briefly the rain retrieval algorithm known as Bayesian Rain retrieval Algorithm Including Neural network (BRAIN). BRAIN is a bayesian-based algorithm described in more details in Viltard et. al (2006). Because rain retrieval using PMR is a ill-posed problem, it is necessary to reduce the number of possible solutions (infinite) to the number physical solutions. Furthermore, within the number of physical solutions associated to a given vector of measured brightness temperatures, there can be a vast number of solutions. In order to overcome this problem, Bayes theorem states that the best estimate in such condition is the average of the possible solutions weighted by their probability of occurrence. In other words if a measured vector of brightness temperature is associated with two solutions 5 and 50 $mm.hr^{-1}$, the “best” answer in the Bayesian sense is going to be a weighted average of 5 and 50 $mm.hr^{-1}$, but closer to 5 $mm.hr^{-1}$ because it is a lot more probable than 50 $mm.hr^{-1}$. Or if one puts it in terms of probabilities, if 5 mm.hr happens 90 % of the time and 50 $mm.hr^{-1}$ happens 10 % of the time, answering 5 $mm.hr^{-1}$ makes you right 90 % of the time and wrong 10 % of the time. The “best” answer in the Bayesian sense is then $0.1*50+.90*5=9.5$ $mm.hr^{-1}$ which makes you wrong 100 % of the time but gives you an unbiased average.

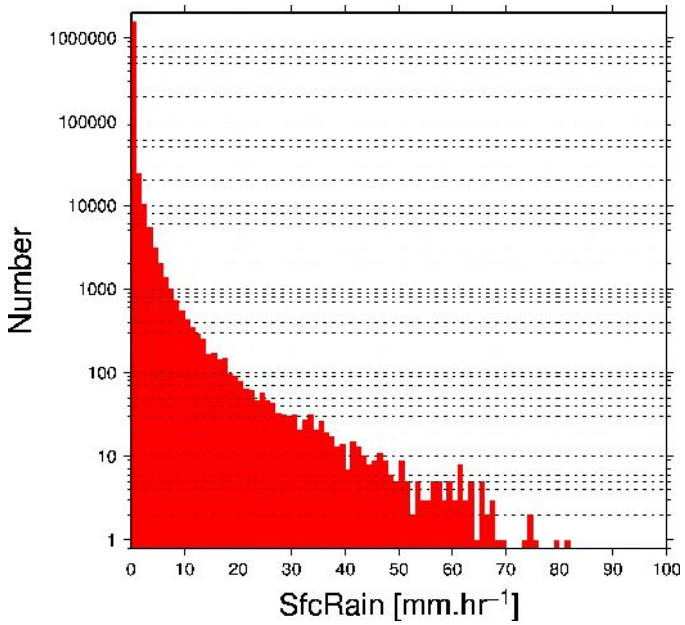

*F**igure 2.1**: Probability distribution of rain rate in the BRAIN database, including the case when RR=0. mm.hr-1. One will notice that low rain rates are much more probable than higher rain rates. This base valid for land surface has 1,650,000 elements among which about 105,000 are rainy.*

To comply with Bayes theorem application, BRAIN uses a retrieval database in which are stored a series of rain rates with their associated brightness temperatures. The retrieval process consists in entering the database space with a measured brightness temperature vector, compute the distance of between each individual in the database and the measurement and average the rain rates of the database weighted by the distance in question.

The fact that the retrieval is based on a Bayesian scheme has a number of important consequences to keep in mind:

-first, the result, when averaged on a “sufficient” number of pixels should be unbiased with respect to the data base. This is true on a global scale if the retrieval database is global.

-second, on a regional or local scale the specific condition of rain can depart from the PDF of the database leading to estimates that are locally biased.

-third, on a pixel-by-pixel basis, the second statement is even more “true” and the performance of the Bayesian scheme could be poor. Luckily, the ambiguity of the possible solutions is not that large and the final pixel-by-pixel estimates is not so bad (we will present later some quantitative results).

***Figure2.2**: Retrieved rain rate in mm.hr^{-1} (left) and associated retrieved convective fraction in % (right) for the same case as presented in **Figure 1.1**. The stratiform and convective regions are well separated in this particularly clear case of continental convection over South America.*

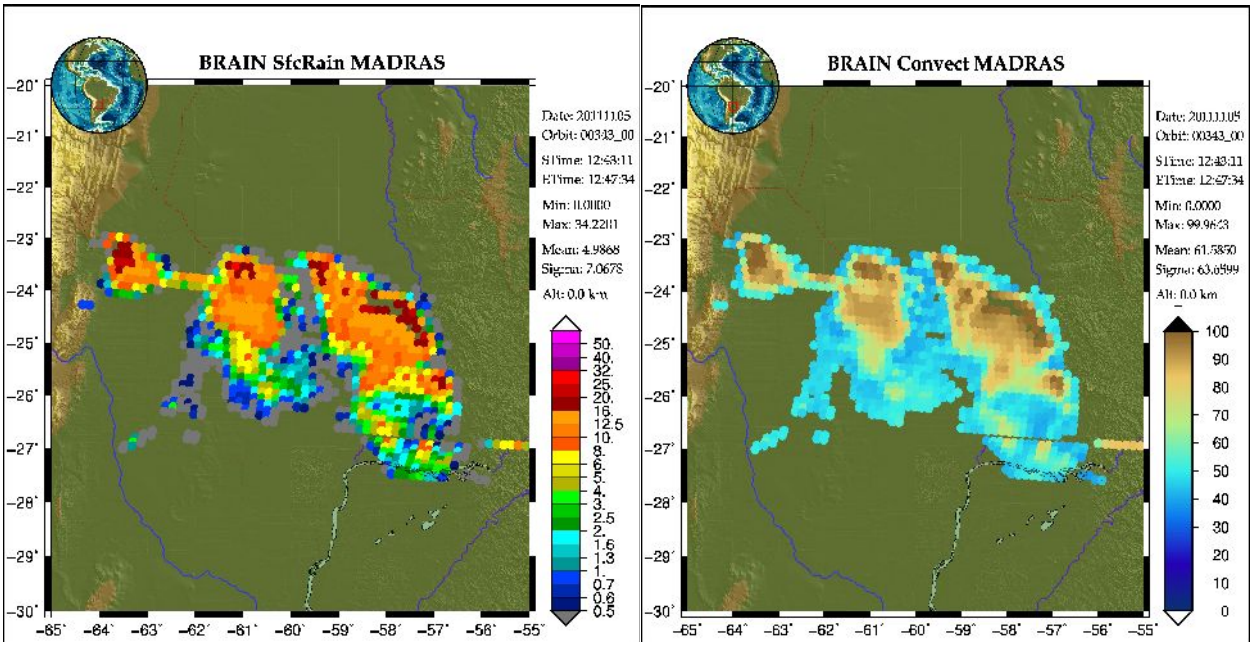

In addition to the intrinsic error of the retrieval itself, if one wants to validate on a pixel-by-pixel basis the retrieved rain field (e.g. with a radar), one should keep in mind that the retrieved rain field is elaborated from the ice phase information and sometimes there can be some parallax effects. In other word, the rain retrieved can be correct but slightly shifted by approximately one pixel but in an arbitrary direction depending on the two instruments angle of view, the configuration of the convection etc... As shown by Berg et al. (2006), this pixel-by-pixel bias and the associated low correlation coefficient improves greatly as soon as some spatial averaging are performed.

From what was explained above, it appears that if one wants to improve the dynamics of the instantaneous rain retrieval, it is necessary to reduce the space of the possible solutions by adding some a-priori information to the retrieval. At the same time, this information must be robust in order to avoid disturbing the Bayesian scheme by favoring elements in the database that should not be. The latter would simply result in introducing a bias in the solution.

3. Database construction and ice microphysics consideration (WP1)

(Collaboration Daniel Vila, Luiz Machado)

The first step is thus to build a data base that will contain elements made of a vector of brightness temperatures and its associated rain rate. To do so, the simplest way could be for instance to co-locate TRMM Microwave Imager data and TRMM Precipitation radar data within the common swath of the two instruments. This was done and presented in Viltard et al. (2006), but then this can only work for TRMM itself since each satellite has a particular configuration in terms of geometry and frequency selection. This means that it will be necessary to be able to simulate brightness temperatures for each instrument's particular configuration. In order to do so, it is necessary to provide the radiative transfer model with a parameterization for the ice particles to simulate accurately the brighntess temperatures, specially above 30 GHz.

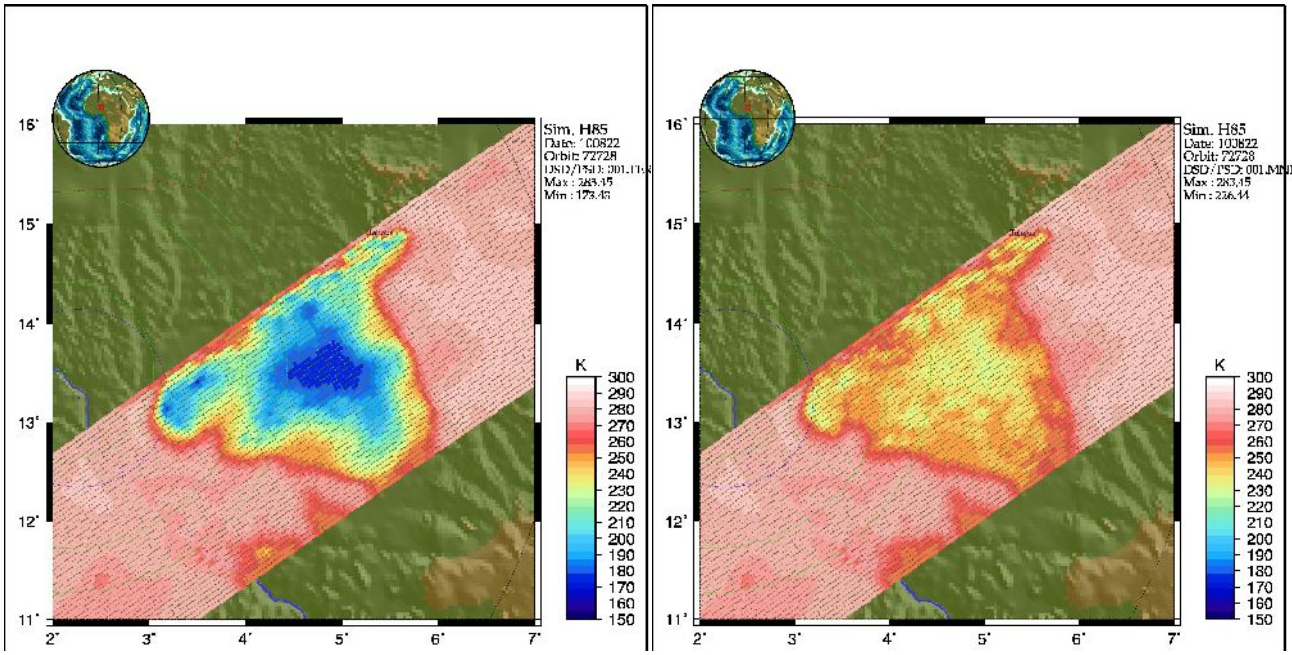

Figure 3.1*: Two simulation of the 85 GHz H on TMI over Africa. The left-hand one is a basic parametrization of ice where snow has a density equal to* ρ*=0.1 g.cm*$^{-3}$ *and graupel has a density equal to* ρ*=0.4 g.cm*$^{-3}$*. The right-hand one is with a more elaborate scheme with different mass-diameter relationship m(D) leading to a density diameter relationship* ρ*(D) for each species.*

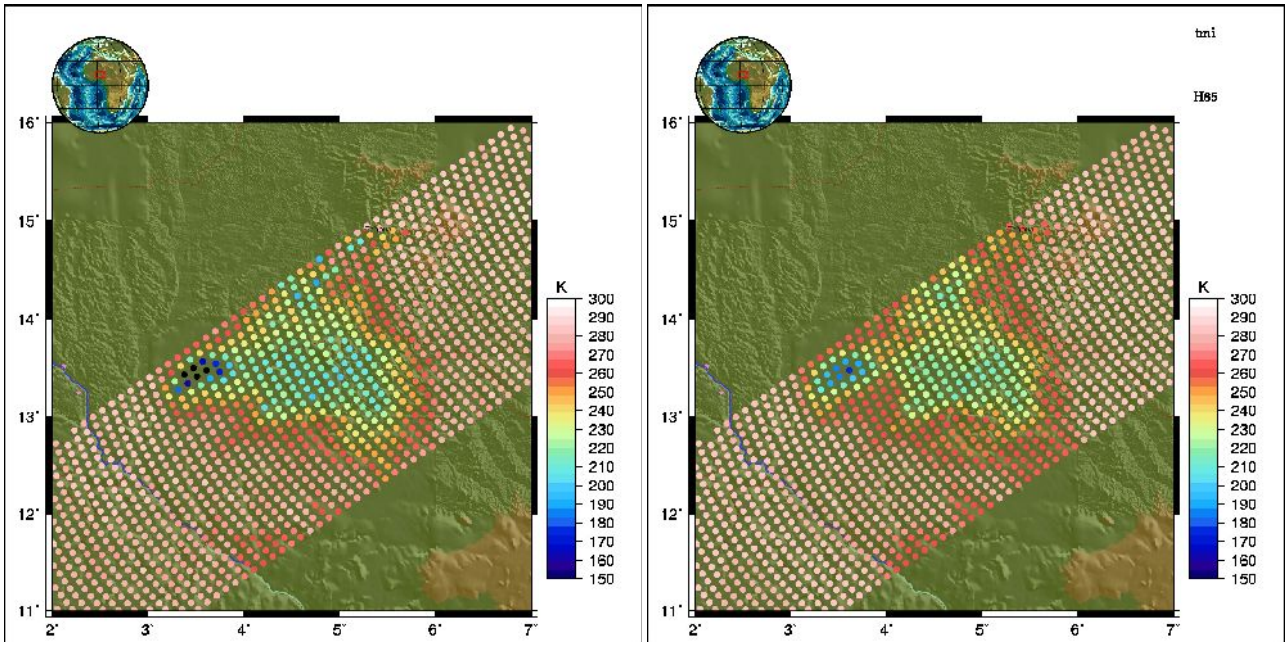

Figure 3.2*: Right hand-side, final simulation with the modified PSD approach, with one species only and a m(D) parameterization deduced from in-situ measurement. Left hand-side, original TMI 85 GHz-H channel brightness temperature.*

Figure 3.1 shows two examples of brightness temperature simulations at 85 GHz in the Horizontal polarization using two different PSD parameterizations in the RTTOV model for a convective system over Africa. The two parameterizations are based on cloud-model values found in the literature (Ferrier, 1994 and Meso-NH Technical Reference Manual, 2008). These parameterizations make a distinction between two species of ice: generic snow which represents particles that are light, fall slowly and grow mostly through water vapor deposition processes and; generic graupel which represent medium-weight particles with faster fall speed and that grow from

faster microphysical processes like aggregation and riming. The main difference between the two images lies in the two type of mass-diameter relationship: the left-hand one ileads to a constant density regardless of the diameter of the particles, the right-hand one is a little bit more elaborated since it gives a different density of particles according to their diameter. It can be seen that neither of them give a satisfactory result when compared to the left-hand side **Figure 3.2**, which is the observed TB at 85 GHz from TMI: the constant density gives way too much scattering in the stratiform region and the variable density lacks scattering in the same stratiform region and also in the convective region. Note that in **Figure 3.1** the simulation are given at the PR resolution, no antenna pattern convolution was applied to enhance the difference between the two ice parametrization.

From the field experiment that we performed in Africa in 2010 in Niger, and following the work of Heymsfield et al. (2010), we found out that it would be more appropriate to only use one species of ice and a unique mass-diameter law. This is based on the idea that as particles will grow larger in size inside the distribution, they will more and more likely be snow-like while smaller particles are denser anyway and closer to graupel-like population. The distinction between the two species being somewhat artificial and definitely driven by cloud model constraints. The resulting simulation is shown on the right-hand side of **Figure 3.2**, where one can see the great improvement over the previous parameterizations. Note that in **Figure 3.2** the antenna pattern was used to compute the "real" pixel resolution of TMI at 85 GHz to emphasize the similarities of structure and intensities.

It is to be noted that we are conscious that the proposed approach is certainly a simplification that work for our application for various reasons. The first one is that the "large" scale we are considering from the microphysics point of view (~10 km) allows us to represent the extreme variability of the ice species with a unique "average" species. Second, the frequency that we use (~37, 85 and 150 GHz) are mostly sensitive to the large precipitating particles in the 5 to 9 km altitude region. Going to higher frequency would mean that we would be more sensitive to a different part of the PSD spectrum and might not work as well.

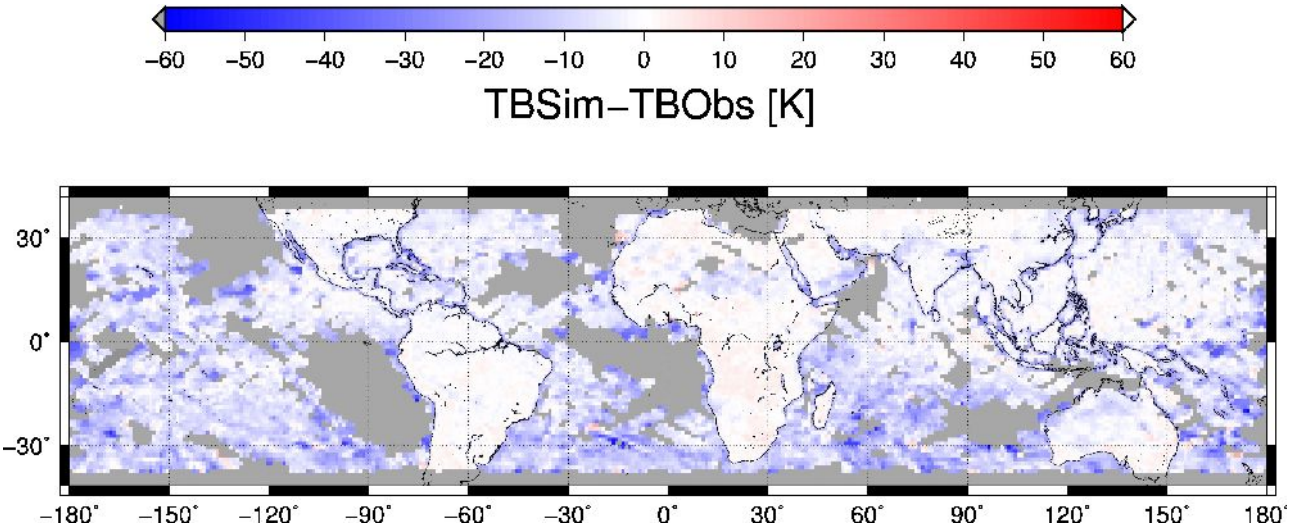

***Figure 3.3**: Error of simulated-observed 85 GHz-H for the point used in the retrieval database for BRAIN. Over land, the microphysical parameterization was adjusted from field campaign. Over ocean, the same parametrization is used, although it was not validated by field campaign. The data are averaged over 1°x1° boxes and represent randomly selected situation over 10 years of TRMM PR and TMI data. There are about 4 millions points.*

Figure 3.3 shows the mean error between simulated and observed 85 GHz brightness temperature over more 4 million pixels of co-located data between PR and TMI, randomly selected from TRMM scenes between 1998 and 2010. The same parameterization was used over land and over ocean,

although we do know that these two should be different. It appears clearly that the error over ocean is much larger than over land, showing the inappropriateness of our parameterization for the former. It can be seen also that the simulated TBs are usually slightly too warm over land and too cold over ocean. It can also be seen that there are regional variability and some continents/ocean are locally differently biased.

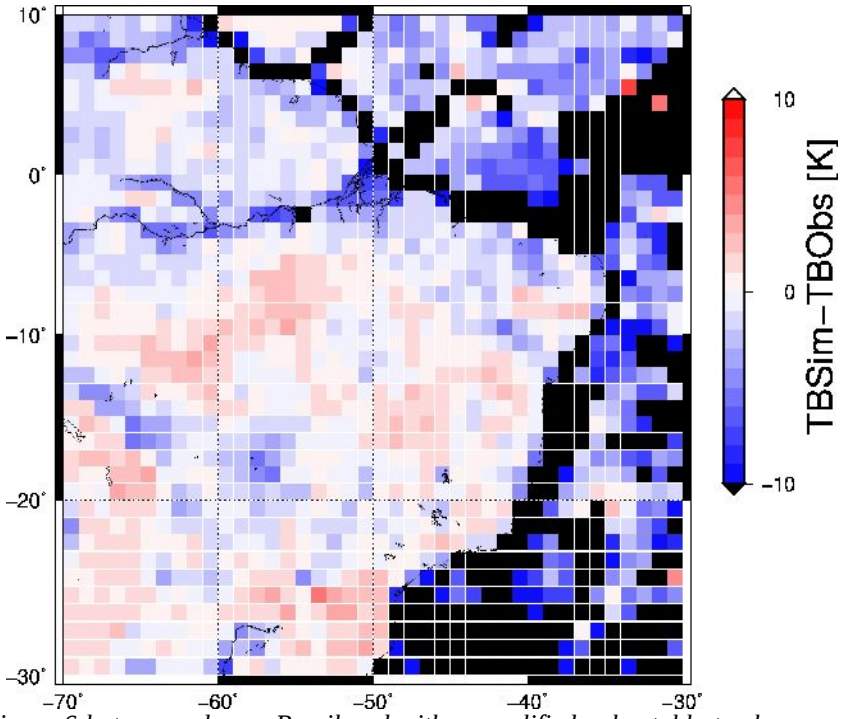

***Figure 3.4**: same as Figure 6 but zoomed over Brazil and with a amplified color table to show more contrast in the regional quality of the simulations. It is to be noted that in scattering regime, an error of 10 K is actually a very good performance. One will notice the systematic negative bias over rivers and lakes.*

Figure 3.4 shows a zoom over Brazil of the **Figure 3.3**. We see that the error between simulated and observed brightness temperature generally below ±10 K and is spatially structured. First, the lakes and river are similarly affected with a cold bias (TBObs > TBSim) which is very likely due to improper emissivity parametrization in those regions. Second the coastal regions are definitely affected by very large error due to the strong transition between ocean and land in terms of emissivity. Third the ocean is also affected by a strong cold bias. Cold bias (TBObs > TBSim) shows that the simulated brightness temperature are too cold, indicating either a improper emissivity value or an excess of scattering. The difficulty here comes once again of the very strong occurrence of light rain and "clear air" with respect to rainy situations, hence the influence of emissivity in the statistics, while in reality the impact of the latter tends to vanish rapidly when the precipitation intensity increases, specially at 85 GHz and above.

A principal components analysis on both observed and simulated brightness temperatures is presented **Figure 3.5**. Each graph represents the contribution of each channel (histogram bar) for each component from the least significant (upper-left) to the most significant (lower-right). In red are the observed brightness temperatures and in black the simulated ones. These components were computed for surface rain rates > 1 $mm.hr^{-1}$ to minimize the surface impact.

It is interesting to notice that there is a very good agreement between simulated and observed components for the 5 most significant components (3 bottom ones, middle-right one and middle one). It is also interesting to see that the first component (explaining 99% of the variance) is

basically the average of all the channels. This is a rather classical result and the simulated Tbs were adjusted to minimize the bias between simulated and observed. The second component is basically the difference between the lower frequency channels and the higher frequency ones. Once again, the very good agreement between simulated and observed shows that we captured most of the dynamics of the emission and scattering. The third component is mostly driven by the de-polarization of the lower frequency channels. This signal comes only in our case from the surface emissivity since we are using spherical particles in the radiative transfer model. Because for the 85 GHz channel the surface is very rapidly obscured by precipitation and we do not simulate re-polarization by scattering particles (Mie scattering), there is not information there in the simulated Tbs. Finally the 4th and 5th component express some more subtle differences between the various channels and are well captured even if the quality is getting lower and lower. It is to be noted that the 37-85 GHz only appear clearly in the last two components which seem to tell us that they do not account for a lot of the brightness temperatures variance.

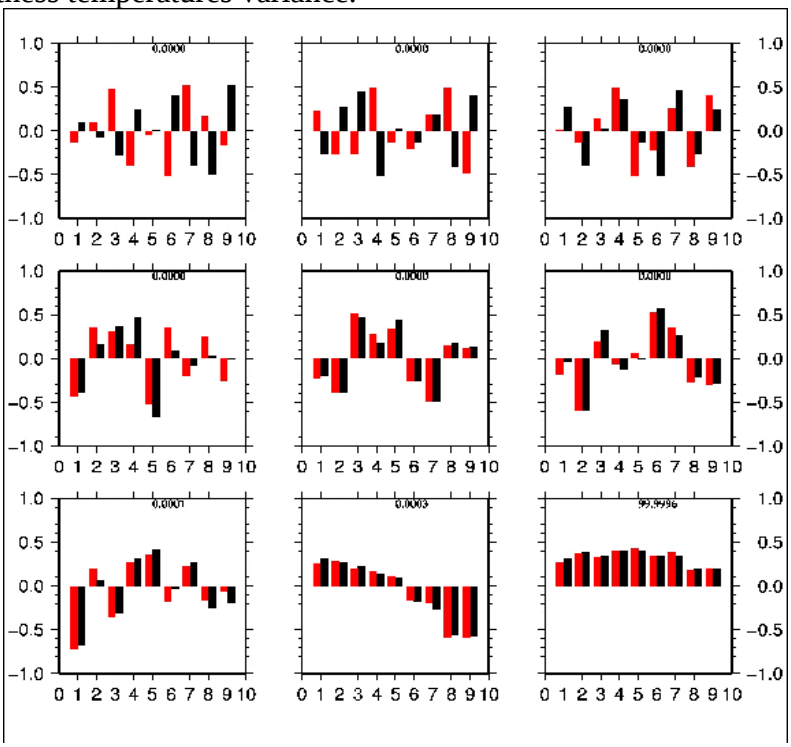

Figure 3.5*: respective contribution of the various Tbs in a Principal Component Analysis over the 9 channels of TMI and over land (about 30,000 points with rain > 1 mm.hr-1). X-axes are labeled from 1 (10 GHz-H) to 9 (85 GHz-V). Y-axis are arbitrary units. The least significant component is in the upper-left corner and the most significant is in the lower right corner. Black bar stand for simulation and red ones for observed* T_B*s.*

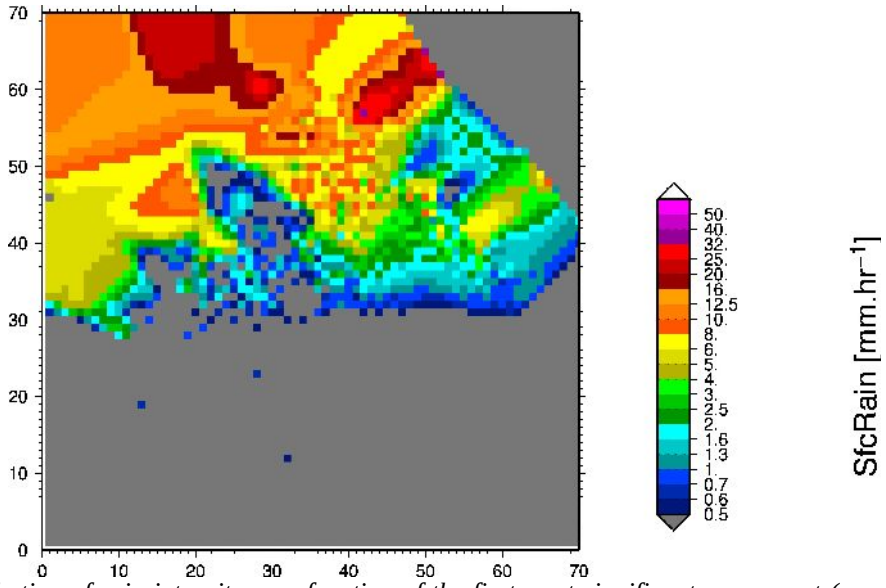

Figure 3.6*: distribution of rain intensity as a function of the first most significant component (x-axis) and the second most significant component (y-axis) as defined in* ***Figure 3.5*** *for TMI.*

Figure 3.6 shows the dependence between the surface rain intensity and the first most significant components of the PCA. It is interesting to note that while the variance of the 9 brightness temperature is vastly explained by the first component 99.99 %, the second component holds quite a bit of information related to the rain intensity, noticeably for discriminating the rainy from the non-rainy situation. This shows that a lot of the brightness temperatures variance is due to other factor besides rain, specially when the rain intensity is low. Interestingly both the **Figure 3.5** and **3.6** are weakly dependent on the considered instrument: TMI, MADRAS (not shown), SSMI (not shown) and SSMIS (not shown).

This new database that was built based on some results from the Niamey 2010 Megha-Tropiques Algorithm validation campaign is a global database. So far there were no in-situ measurement of ice properties during the CHUVA campaign. Hence to build a specific ice scheme over Brazil would require to use the ground-based radar particles identification as presented in the following **Part 6**. Nervertheless two questions can be raised at that point: first, the particle classification from the radar does not give a lot of information about the actual mass-diameter law of the ice. It gives a qualitative idea of the type of particles that can be found in a particular region of the system. Second, the variability (at the considered scale) of the mass-diameter law does not seem so critical. The errors between simulated and observed TBs are rather homogeneous over all the continents while the M(D) used was measured in Africa for stratiform regions. The modulation of the error seems more affected by improperly set surface emissivities than by improperly set mass-diameter laws (except in convective areas obviously). In **Part 6** we will discuss further how we plan to improve that particular aspect in the near future using the CHUVA data.

4 BRAIN performance assessment over Brasil (WP2-WP4)

We do here a comparison using the common swath between TMI and PR (100 km on both sides of the sub-satellite point. This allows us to co-locate the rain from PR and the rain from BRAIN particularly after averaging the PR at BRAIN resolution: 12 km circular pixels while the native resolution of PR is about 5 km. Because we're working only with the center swath of TMI, the sampling is not as favorable as with the full swath and we have to be cautious about

representativeness. In order to minimize this effect, we will also present the results in 1°x1° degree grid-boxes.

Note that this version of BRAIN that was developed during the 6 month visit with the idea that we should try to improve warm rain retrieval, IS NOT in its finalized version, specially when it comes to final adjustment of the retrieval weightings. Thus, these results should be seen as preliminary, demonstrating the potential of the algorithm rather than its final performances.

Figure 4.1 shows on the left hand side the number of pixels per 1°x1° boxes for November 2011-February 2012. It shows that most of the boxes contain about 5000 pixels, except in the southernmost region where the number increases to about 10,000 and then drops when one reaches the very edge of the PR/TMI common swath. The right hand side of the same **Figure 4.1** shows the classification of the surface type as land/ocean/coast. Regions where only ocean pixel are found are classified as “ocean”, region where only land pixel are found are classified as “land”, and regions where mixed pixels are found (either land, ocean or coast) are classified as “coast”. One has to remember that the ocean and land pixels are retrieved respectively with a particular configuration of BRAIN. Since they are homogeneous, the statistics are given for a given configuration of BRAIN over these two surface types. For coast, three different configuration of BRAIN can be found in the same box and thus statistics are more difficult to interpret.

Figure 4.2 represents the 1°x1° average rain retrieved for PR (left-hand side) and BRAIN (right-hand side) in $mm.hr^{-1}$. One has to remember that this is not the accumulation of rain over the four month under consideration since there is a large bias due to the poor satellite sampling. If these images can be interpreted physically they would be somewhat a estimate of the average rain rate observed by the two instruments over a 4-month period when, and only when, there where overpasses. The only aspect here that can be considered is the fact that the two instrument did sample the same systems, the same number of time and hence the direct comparison between the two rain rate can be used to assess the BRAIN performances to retrieve instantaneous rain, assuming PR is a reference.

One other aspect of rain that makes things difficult when validating is the fact that rain is an intermittent field as stated earlier. We can assume here that the temporal intermittence is under control here since we have two measures at about 1 minute interval, but the spatial intermittence is still present and the capability to detect rain for the two instruments is different. This combines with the fact that the null rain ($RR = 0. mm.hr^{-1}$) is much more probable that $RR > 0\ mm.hr^{-1}$, leading to the fact that the rain/no-rain delineation will be of critical importance. On the other hand, we know that PR has a detection threshold due to hardware constraint close to 17 dBZ (Kummerow et al. 1998). This leads in theory to a minimum rain detection of about 0.1-0.2 $mm.hr^{-1}$, but in reality literature (see for instance Berg et al. 2010) shows that a robust minimum is probably closer to 0.8-0.9 $mm.hr^{-1}$.

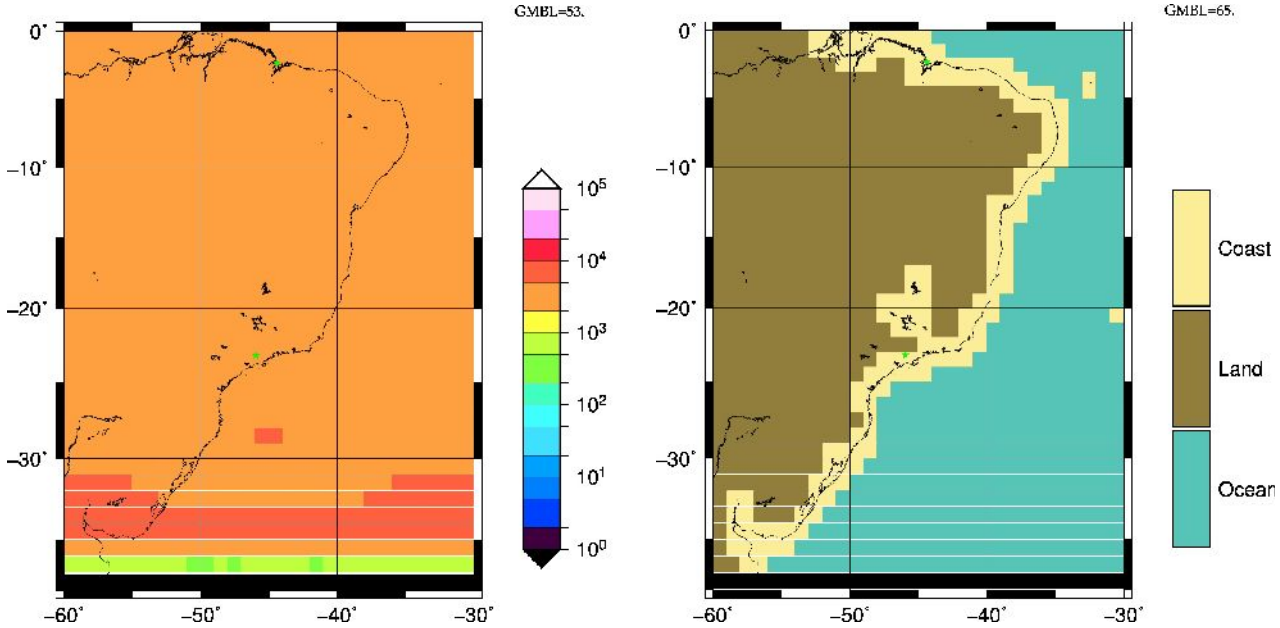

Figure 4.1: right, distribution of the number of pixels per 1°x1° grid box for 4 month of data (November 2011 to February 2012). Left, surface type classification over the region of interest. The two green stars are respectively the Alcantara and the Vale do Paraiba location of the X-band radar.

On the other hand, BRAIN provides a probability of rain along with the rain rate. The probability is represented by a number that follows an inverse Gumble distribution. This number varies from 50 to 100 %. 100 % means that the rain is certain, while 50% means that rain is unlikely. The following rain field will always be presented with the associated threshold that was chosen, meaning that pixel with a probability below the threshold will be considered as non-rainy and above the threshold will be considered as rainy. The inverse Gumble distribution has a sharp edge and thus experience shows that a threshold value between 57 and 65 % usually gives the best agreement between PR and BRAIN.

Threshold	Hits	Total
57.	0.187 (+6.7 %)	$-1.42\ 10^{-2}$ (-9.5 %)
65.	$-6.53\ 10^{-2}$ (-2.8 %)	$-1.21\ 10^{-2}$ (-8.64 %)

Table 1: Bias (and Error) in mm.hr^{-1} (%) for all surfaces computed at pixel level and for the region showed ***Figure 4.1****. "Hits" stands for pixels when both instruments saw rain, "Total" counts all the pixels for each instruments.*

Threshold	Hits	Total
57.	-0.21 (-15 %)	$-3.12\ 10^{-3}$ (-36 %)
65.	-0.38 (-29.9 %)	$-2.91\ 10^{-2}$ (-34 %)

Table 2: Same as Table 1 but for Land only.

The average rain rate of the land database is about $6.0\ 10^{-2}$ mm.hr^{-1} (including RR = 0. mm.hr^{-1}) and in theory if we average globally the output of BRAIN over a long enough period of time, the average surface rain should tend toward this value. Nevertheless as pointed out previously, the regional biases could be large and the bias between the simulated and the observed brightness temperature will also have an influence. Since our database was built from a large number of PR surface rain estimates, if accumulated over a large enough number of point, the BRAIN retrieval and the PR estimates should converge at global scale.

Table 1 shows the bias at pixel level for the domain of **Figure 4.1** and further. Because the influence of RR = 0 mm.hr^{-1} is so strong on the rain average, we distinguish between the "Hits" case and the "Total" case. The "Hits" are those pixels when both PR and BRAIN did see some rain (RR > 0 mm.hr^{-1}), the "Total" case is when we compute the rain average where we have a PR and a BRAIN co-located pixel. The number of "Hits" will unfortunately varies with the chosen threshold because some BRAIN light surface rain might be with a low probability of rain but with a positive rain rate nonetheless.

As stated before, **Figure 4.2** shows the 1°x1° average rain rate for the November 2011-March 2012 period for PR and BRAIN respectively. Over ocean, a lot of features are very similar in terms of both intensities and structures. The maxima are properly located and the North-South gradient is well described. Over land on the other hand a systematic low bias can be seen in BRAIN. This underestimation has various sources. The first one and most probable is the fact that the present version of BRAIN hasn't been totally optimized and the weightings could be improved to at least reach the performances found in Kirstetter et al. 2012 over Africa. Second, it seems that the current version of BRAIN has a difficult time detecting the proper rain/no-rain limit in a number of cases as the following skill score will show.

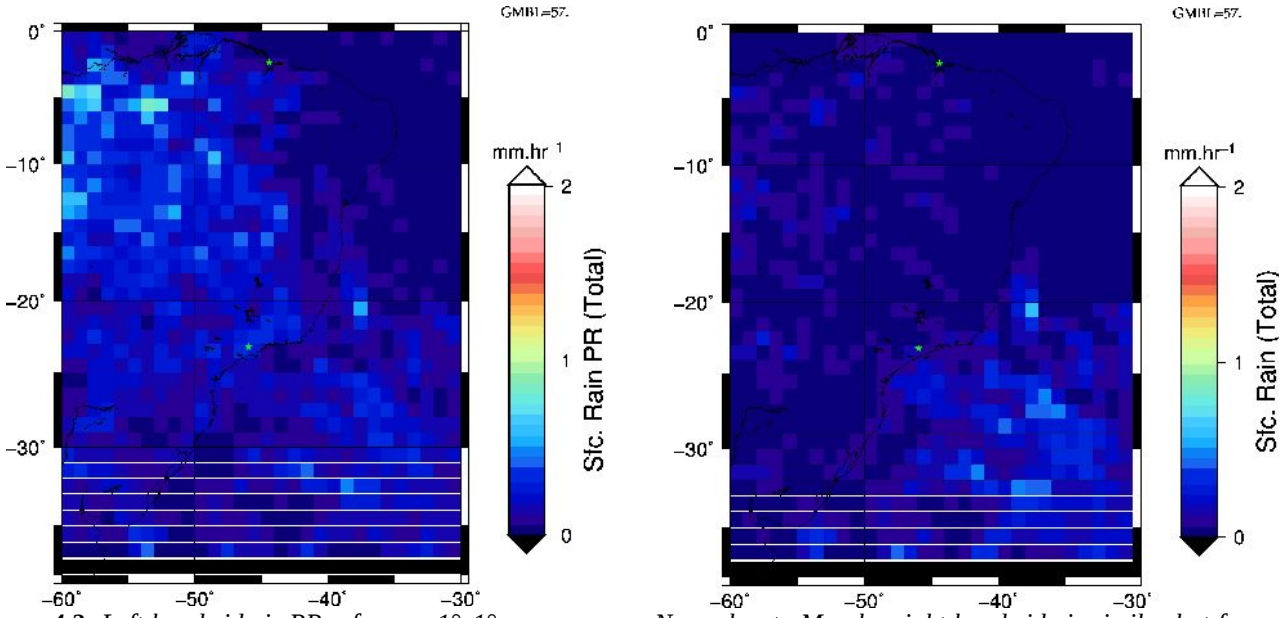

***Figure 4.2**: Left hand side is PR reference 1°x1° average over November to March , right hand side is similar but for BRAIN retrieval. THESE ARE ONLY MEANINGFULL TO BE COMPARED TOGETHER.*

The **Figure 4.3** shows the Heidke Skill Score (HSS) for two different Gumble Threshold. The HSS measures the quality of a forecast (here, rain/no rain), summarizing somewhat the contingency table. HSS of 0 shows no better skill than random, negative shows worse skills and positive is an improvement with respect to random. HSS of 1 is perfect forecast. From this figure, it is clear that the optimal Gumble threshold are different over land and ocean. Over ocean, a higher values for the inverse Gumble threshold is permitted which leads to good skill score particularly in the South and the Northernmost part of the domain. Over land, the HSS is better when a lower threshold is applied showing that detection of rain is more difficult over land. At the same time, this increase in the HSS is somewhat artificial over land as choosing a 51 % threshold gives almost rain in every pixel and hence leads to a strong underestimate of the rain by BRAIN by adding many small rain rates. This could be worked out in the near future by using the radar data from the various CHUVA campaigns to adjust regionally the most adequate Gumble threshold. It is important though, that the radar data be of very good quality in order to remove all false alarms (ground clutter, partial beam

blocking etc...) that mau lead to inaccurate or improper rain/no-rain detection.

It can also be seen from **Figure 4.4** that there are two very distinct trend between land and ocean. Above ocean, where BRAIN makes use of all the available channels at the same time, we tend to overestimate the rain intensity while above land where we use only the scattering channels (37V-85H-85V), the trend is clearly to underestimate the rain intensities. This is clearly shown in Table 2 also where the error above land at pixel level (~-35 %) is much larger than the global error shown Table 1 (~-9 %).

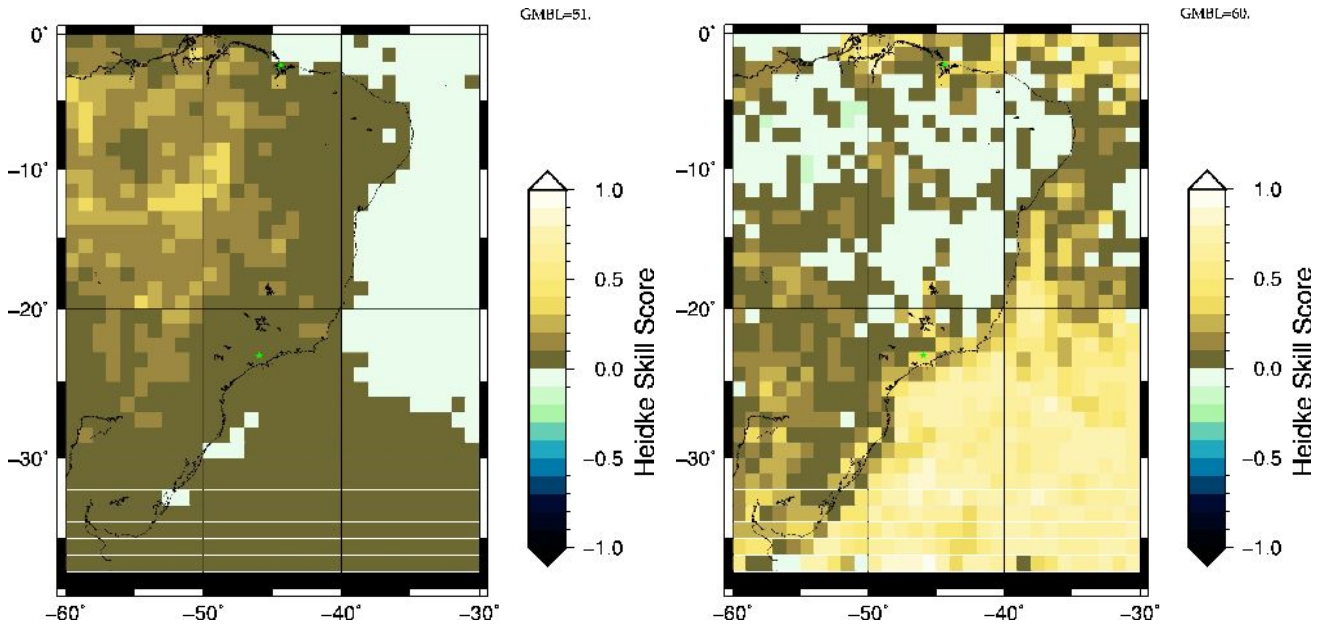

***Figure 4.3**: Heidke Skill Score for a Gumble of 51. (left) and 60. (right)*

Threshold	Total Land	Total Coast
57.	-7.39 10^{-3} (-21 %)	0.99 (+990 %)
65.	-6.82 10^{-3} (-22 %)	1.00 (+909 %)

Table 3: Same as Table 2 for Land and Coast but at a 1°x1° resolution instead of pixel resolution and only for the Total rain.

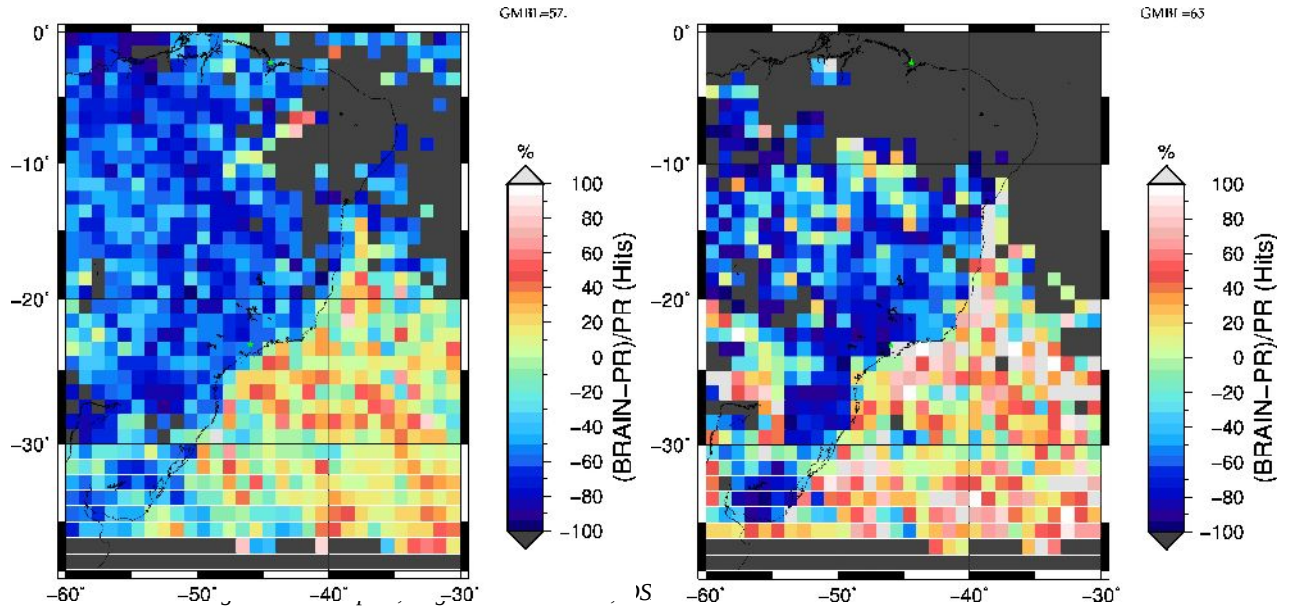

Figure 4.4*: Influence of the threshold of rain probability on the relative error between BRAIN and PR. On the left-and side, a threshold of 57. %, on the right-hand side a threshold of 65. % The left-hand side figure corresponds to the* ***Figure 4.2****. The larger the threshold, the less pixels are considered rainy.*

Table 3 shows the same kind of results as Table 1 and 2 but for 1°x1° grid boxes average and only for land and coast. Coast is defined as a 1° box that has a mixture of land and ocean pixel in it. When averaged, the performances improve because part of the error is due to the over/under estimation of the rain radar from BRAIN but a lot of this error is due to the fact that the two instrument do not put the rain exactly at the same location. This is due mainly to the fact that ice signature can be shifted through wind shear and horizontal advection with respect to the maximum rain, not mentioning the possible tilt of the convection itself. In addition, the PR is cross-track looking and TMI is looking at a 50° zenith angle. Finally, the TMI is sensing the integrated ice content with a peak sensitivity at about 6 to 9 km altitude. Hence there is a shift of roughly 6 to 9 km between the maximum detected scattering region and the real location of the maximum rain. Because all these geometric aspects are very random depending on the situation, they are impossible to correct. When averaging spatially, the co-location error goes down because at a 1°x1° resolution these effects are negligible.

The performances of this version of BRAIN at 1°x1° are slightly below -20 % over land. This performance could probably be taken closer to 10-15% (absolute value) with more optimized retrieval weights and an improved threshold on the rain/no-rain detection. This will be done over the next few month, using in particular the radar data once processed properly.

Table 3 also shows the performances over the coastal areas where the retrieval is extremely difficult because of the strong heterogeneity of the surface properties. Even the channels the less affected by surface (85 GHz) are affected by this dramatic change of emissivity. Hence, very large errors are shown in the retrieval for this version of BRAIN. Over coastal areas, this version of BRAIN uses the same algorithm as the land areas.

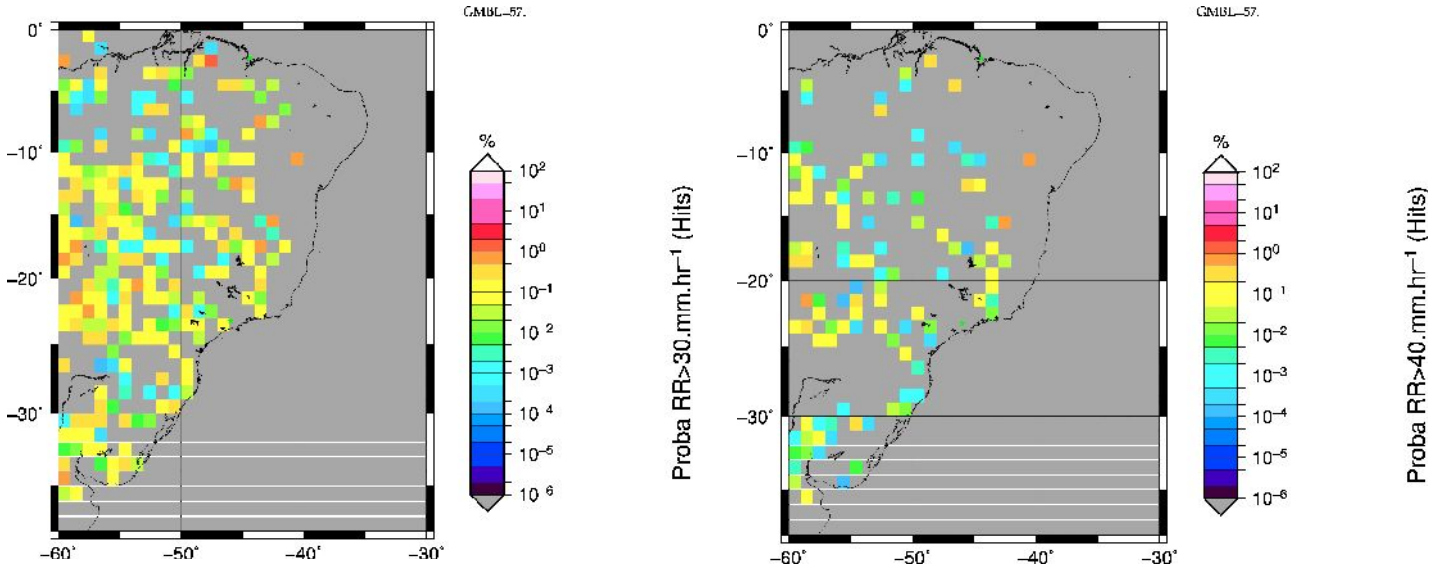

Figure 4.5*: probability of rain rates above 30 mm.hr^{-1} (left) and above 40 mm.hr^{-1} (right). The values over ocean are non-relevant.* THESE ARE PRELIMINARY RESULTS.

Figure 4.5 shows the average probability of rain to be above a certain threshold. BRAIN computes the rain rate as the weighted average of the neighboring rain rates in the retrieval database. The weights are based on the distance between the measured vector of T_Bs and each element of the database. In other word, as stated above, when giving only the expected rain rate, one does not extract all the available information from the Bayesian scheme or its associated database. It is then possible to compute the probability of rain above a certain value by summing all the weights of the rain that is above the considered threshold. In the example of Figure 4.5 two different threshold are shown, the probability of rain over 30 mm.hr^{-1} and the probability of rain over 40 mm.hr^{-1}. The regions that have a significant probability of rain above 30 mm.hr^{-1} are scattered over Brasil, although they do not seem to be randomly distributed. They are found mostly in the regions where one expects the highest rain rates to be found noticeably in the Northern part of the country (2.5 S-50W) and in the central region. When one looks at the 40 mm.hr^{-1} probability, the regions of occurrence are much reduced with a concentration of probabilities in the South where active convection is associated with the frontal activity, in the center where active convection is almost always active and in the North where you expect the seasonal influx of oceanic air. These results are preliminary as they would need to be more precisely compared with the convective activity as seen by ForTraCC (see ref below) for instance.

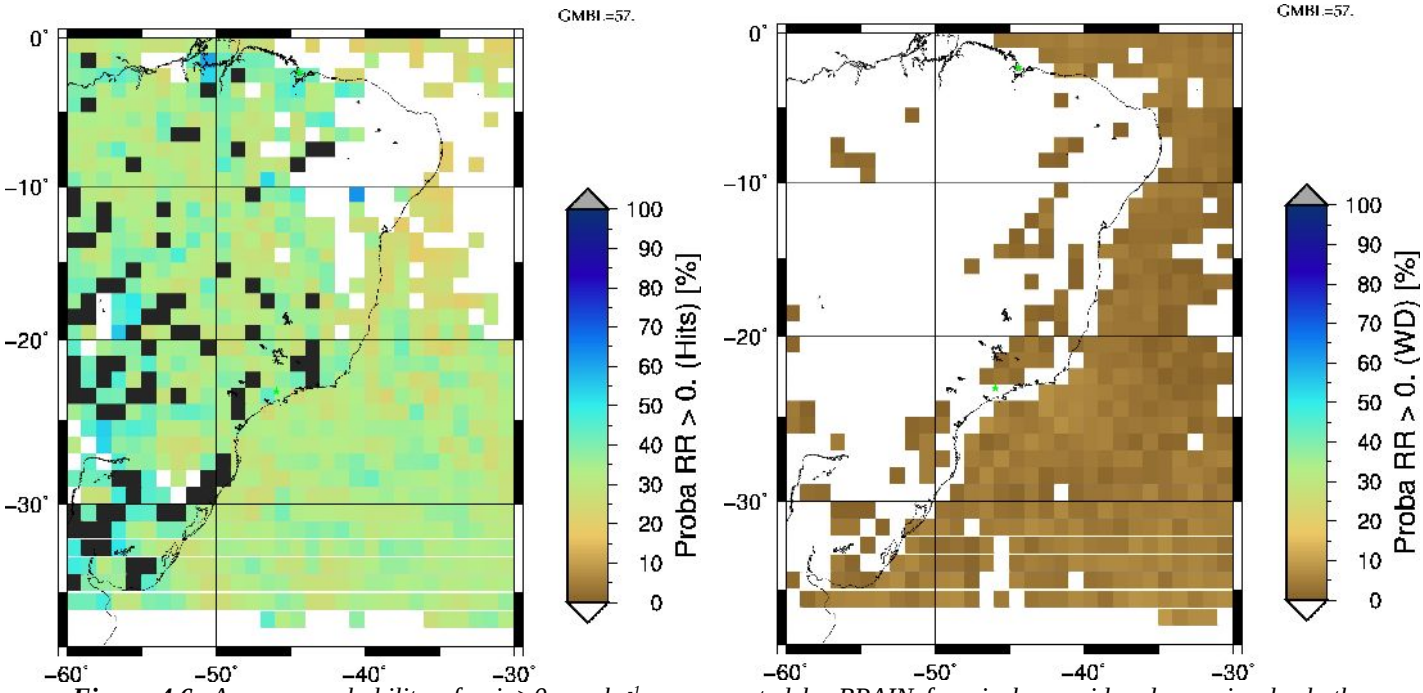

***Figure 4.6**: Average probability of rain>0 mm.hr^{-1} as computed by BRAIN for pixels considered as rainy by both BRAIN and PR (left) and for the Wrong Detection (BRAIN=0, PR >0) (right).*

Figure 4.6 shows as a preliminary result the probabilities of rain positive computed from BRAIN for the Hits case (see above) and the Wrong Detection case. The probability is computed as the average Gumble value found within each 1°x1° box (brought from [50 %,100%] to [0%-100%] for readability). Since the inverse Gumble value defines the rain/no-rain, it is interesting to see if hit situation are indeed consistent throughout the whole domain or if they vary regionally, showing that the rain definition might be locally changing due to different regimes or different brightness temperature signatures. It can be seen that the average values over ocean are quite homogeneous, with no apparent gradient between the North and the South, indicating that we are not very much affected by sea surface temperature (connected to the surface emissivity above ocean). On the other hand, the land case is more contrasted with some regions where the surface emissivity might play a role (Amazon river) and other regions where may be the rain regime/scattering signatures play a role in defining the rain/no-rain determination.

More important though is what is seen for the Wrong Detection. The Wrong detection are those situation where PR has detected rain and BRAIN has not. Supposedely, the warm rain situation should fall under this class as they have a weak or no signature in the brightness temperatures but should be nonetheless detected by PR (at least in the central region of the swath where not affected by the ground cluttering). It appears that over ocean, the probability of rain is extremely consistently low, showing our good score over such surface. Note nevertheless that the Threshold for rain/no-rain is here of 57% which means that a lot of pixels are considered rainy. Over Land, where PR detects rain and BRAIN doesn't, most of the time it seems that there is no way that BRAIN can see anything because the rain probability for these case is mostly 0 except for a few isolated regions and some larger patches in the Southern coastal regions.

It is somewhat disappointing that BRAIN is unable to affect a positive probability to warm rains situations, whatever weak it could be. It seems from these preliminary results that there is no signal in the brightness temperature over land or in the coastal region of rain when warm rain is present. It is true though that warm rain are often coastal in Brazil which makes them twice as hard to detect, but we had some hopes that may be at least the rain probability would be slightly above 0, allowing to affect a rain rate in such cases. We will try in the future to find a number of documented cases from CHUVA radar data where we have at the same time an overpass of PR and TMI to see if PR is indeed capable of detecting these warm rains because, if not, our statistics here fails not because of BRAIN but because of PR !

5 Life Cycle and microwave (WP3)

(collaboration Wagner F. Lima, Luiz A. Machado)

The combination of microwave and tracking information from infra-red geostationary satellite was at the base of this proposal. As presented in the introduction, on the one hand, we know from many studies (e. g. Houze, 1993) that the dynamics and the microphysics of cloud and precipitation evolve throughout the life cycle of the systems. Since there is on degree of freedom too many between T_B, ice content and ice species, the information about the life cycle phase of the system was foreseen as relevant to reduce the ambiguity. Basically, for a given vector of measured brightness temperature, we would expect the surface rain to be different if we are looking at a early convective cell, a large mature system or a long-lived stratiform blob.

We used the ForTraCC (Vila et al. 2008) tracking system to assess the life cycle of the systems from the GOES satellite infra_red data, and the TRMM TMI and PR data for the passive microwave brightness temperatures and the rain reference respectively. The statistic is built using the co-location of TMI data and the ForTraCC information over the November 2011 to March 2012, while the CHUVA VAP field experiment is going on.

We define the normalized life cycle so that all system start at 0 % and dissipate at 100 % by dividing each time step by the the total duration of the system as computed by ForTraCC. Rather large filtering was needed in order to extract the convection life cycle and keep only those systems with a well defined developing stage, mature stage and dissipating stage. Splitting and merging of systems were filtered out. Large systems, likely to be associated more with frontal system for instance were also filtered out. System which duration is less than 3 GOES images are also disregarded and system with a beginning or an end size larger than 350 pixels are suspicious and were also filtered out.

We focus here on a limited region including the CHUVA Vale do Paraiba radar: 15 South, 31 South,

37 West and 57 West. Another study is under way on a box including the northern part of Brazil and Amazon where we expect eventually a convection with a better defined life cycle.

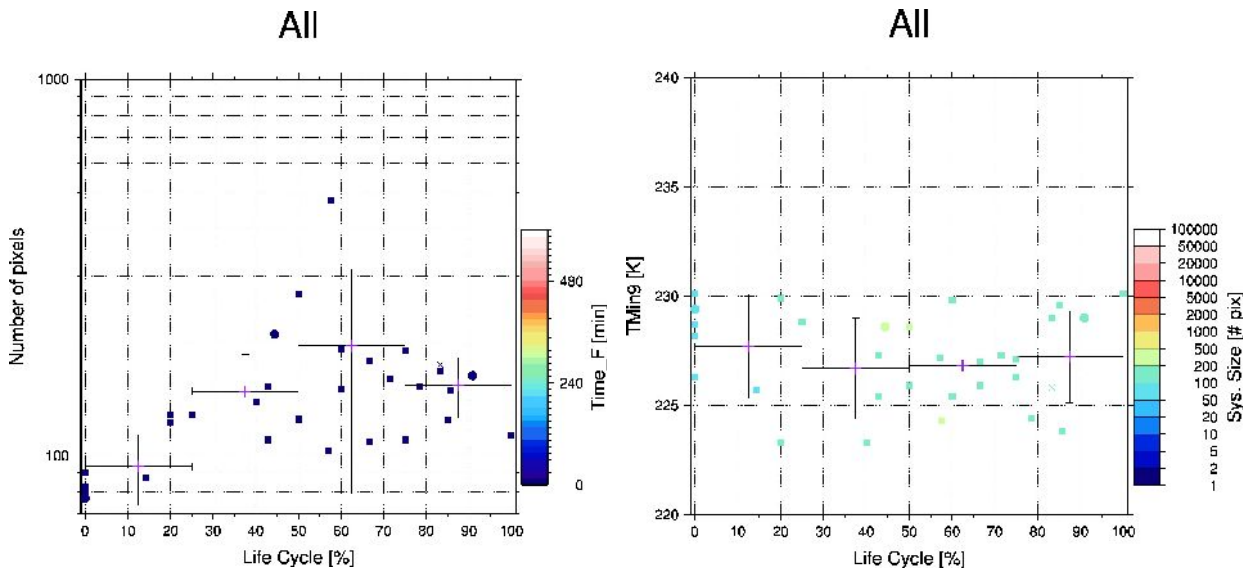

Figure 5.1*: ForTraCC information for November to March 2011 centered on over the CHUVA site "Vale do Paraiba". Left-hand side is the average size of the system as a function of the normalized life cycle. Right hand-side is the evolution of the 9 coldest IR TB pixels as a function of the normalized life cycle. On the left the color of the points indicates the total duration of the system in minutes. On the right the color indicates the maximum size reached by the system during its lifetime in number of pixels.*

Figure 5.1 shows the average trend of the 9 coldest pixels (right) and of the average size of of the systems as a function of the normalized life cycle. These results are pretty classical and are meant to check that our filtering is effective. As expected, the systems reach their maximum size at about 60 % of their life once the convection has stopped or is decaying and the spatial extension is largely due to horizontal advection of ice particles in the stratiform region. At the same time, the coldest IR TB is reached at the end of the convective activity around 40 % of the life cycle. Then the falling ice cloud will tend to warm up the system globally. One can notice that the dispersion of the points is high, indicating a important spread of the various convective situations around the average model.

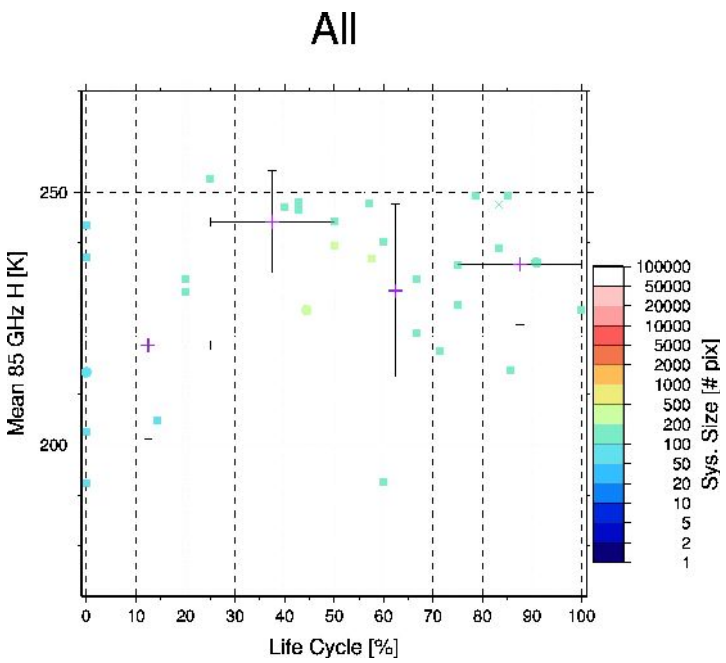

***Figure 5.2**: Evolution of the 85 GHz Horizontal polarization of TMI as a function of the systems' normalized life cycle. The color of each point indicates the associated maximum size reached by the system The color of the dots indicates the maximum size reached by the system in number of pixels.*

Figure 5.2 shows the evolution of the mean T_B 85 H as a function of the normalized life cycle. A rather direct signature of the microphysics effects can be seen on this picture. First, while convection is active in the first 20 % of the system's life, the dense particles dominate with graupel-like ice being generated in the sustained updrafts. These particles will quickly fall down and melt to contribute to the intense rain associated with the convective cells. Some lighter particles will be also produced in the convection and these particles will be horizontally advected and create the stratiform region. As the region develops these particles being dominated by snow-like particles will produce warmer T_Bs which will contribute to warm the average brightness temperature around the 40 % of the life cycle. This is due to the fact that at the mature stage, the startiform region is much larger than the convective region.

Once the convection stops, around 60 % of the life cycle, and as the time goes by, slow microphysical processes (e. g. vapor deposition) will tend to increase the size of the snow flakes leading to an increase of the scattering in the stratiform part. As these crystal grow they tend to fall also and accretion processes will also tend to increase their size, increasing again scattering. Because no new crystal are produced (few in fact in the mesoscale updrafts associated with the stratiform region, see Houze 1993), all the snow flakes tend to fall down as the system slowly collapses. Only the light and small flakes remain, leading to an increase again of the average brightness temperature at the 90 % of the life cycle.

One will notice that no apparent difference or correlation between the average T_B 85 GHz and the maximum size of the system seem to be observed. Nevertheless, it is important to remember that large system have been filtered out to eliminate any non convectively driven clouds like frontal systems.

This is also a somewhat disappointing result in the sense that it does not seem possible to use the a priori information from ForTraCC to constrain BRAIN retrieval. The comparison of ForTraCC and the 85 GHz brightness temperature tell us quite a number of information about the microphysics of the cloud though. This will be consolidated in the near future but there is a good consistency

between our knowledge of such processes and the life cycle detected from the IR data. The wuestion that arises now is : why doesn't the life cycle signature correlates better with the brightness temperature in a manner that would allow us to characterize more directly the surface rain rate ? The first reason comes probably from the fact that it is difficult to define the life cycle for individual systems. A lot of the observed system experience split and merge during their life and as such do not have a clear definition of what is a life cycle. So, in the first place, this particular aspect should be improved in our use of ForTraCC. Second, we might have performed our test in a region where most of the rain is not necessarily convectively driven. A substantial part of the rain over Vale do Paraiba is actually driven by frontal activity coming from the South and for which a life cycle is also hard to define. We are thinking about testing the concept over the Amazon region where may be convective cells are easier to define. But that means also that the ForTraCC information might be usable only in a limited number of situations and thus used with caution because it could induce some serious regional biases. This will be investigated in the near future as it is a key aspect to improve rain retrieval from passive microwave radiometers.

6. Particles classification

(collaboration Thiago Biscarro, Luiz A. Machado, Audrey Martini)

This part is a more direct use of the CHUVA data. We know that the X-band radar that was deployed in CHUVA has a polarimetric capability. Using the combination of the various polarimetric variables measured by the radar, it is possible to asses to a certain extent the type of particles that were observed within a given radar bin. Abundant literature can be found on polarimetric radar techniques and more specifically on Particles Identification (PID), a good reference being Vivekanandan (1991). The general principle of PID is to use a fuzzy logic approach to combine the information brought by the various polarimetric measurements in order to come up for each radar bin with a particle type. Through simulation of direct measurements, a number of particles signatures are identified. The number of “species” is limited from 10 to 20 for practical reasons and for each of these species for each of the radar bin, the fuzzy logic algorithm actually provides a probability. Then, usually the most probable species is kept as being the species in the radar bin.

We will not get here more into the details of particles classification but we are interested in testing if the radar PID can be somewhat correlated to the 85 GHz brightness temperature in order to explain the effect of particles density and the ice content on the scattering.

We used here the PID software provided by GEMATRONIC owner and builder of the X-Band radar deployed in CHUVA. In this software named ECLASS (Echo CLASSification), various PID parametrisation can be found, we used the one proposed presented as “BMRC algorithm for C band” (Keenan, 2003). This version was originally developed for C-band but makes use of polarimetric variables that are not frequency dependent except for KDP (Specific Differential Phase) which is automatically adjusted in the ECLASS software.

Figure 6.0 shows a direct comparison between the reflectivity seen by the X-band radar and the PR at 7 km altitude. One can see the excellent match in terms of structure and location of the maximum. One can also notice that there might be a slight over-correction of attenuation in the outer rings of the X-Band radar further than 70 km, specially in the North and East quadrant. Be aware nonetheless that the two instruments are in their native resolution and that the X-band radar should be downgraded to 5x5 km^2 to match exactly the PR resolution. This difference in resolution might also explain the difference in maximum reflectivity (40 dBZ for X-band, 32.6 dBZ for PR) but a more thorough investigation to check that there is not a small calibration offset of the X-band.

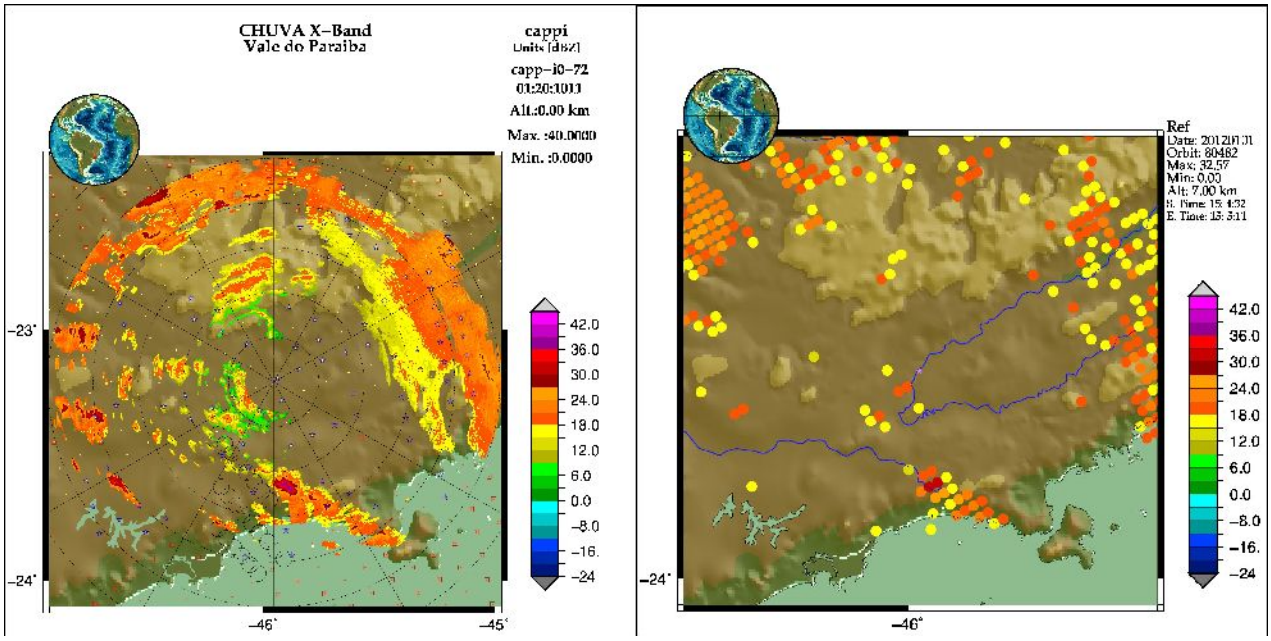

Figure 6.0: *horizontal cross section of reflectivity in dBZ as seen by the X-band radar of CHUVA-VAP and TRMM-PR at 7km altitude on January 1st 2012 at 15h05 UTC. The same color table is used for both images although it is not optimized for the rather low sensitivity of PR (17 dBZ) when compared to the X-band.*

An example is shown on **Figure 6.1** for a PPI at 4.6° elevation at 15:00 UTC on January 1st 2012 during CHUVA Vale do Paraiba. We chose this event because at the same time, TMI was overpassing the radar. At this elevation and since the radar altitude itself is about 700 m, the freezing height is met at about 43 km from the radar. Between the radar and this distance the main particles type are a mix of drizzle and wet graupel. The wet graupel are probably melting ice particles that persist through the freezing level.

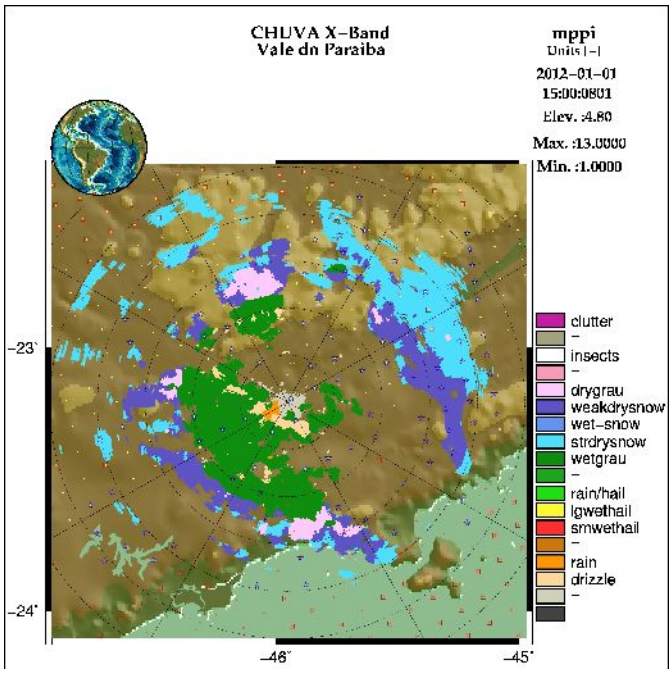

Figure 6.1*: example of a PID for a 4.60° elevation Plan Position Indicator at 15:00 TU on 1st of January 2012. See text for explanations. Each of the dashed concentric circle is 20 km distance from the radar.*

At farther distance, we enter the cold microphysics and get mostly wet snow just above the melting layer and then dry snow above. There are also a couple of dry graupel spots in the North and the South of the radar and smaller areas East and West.

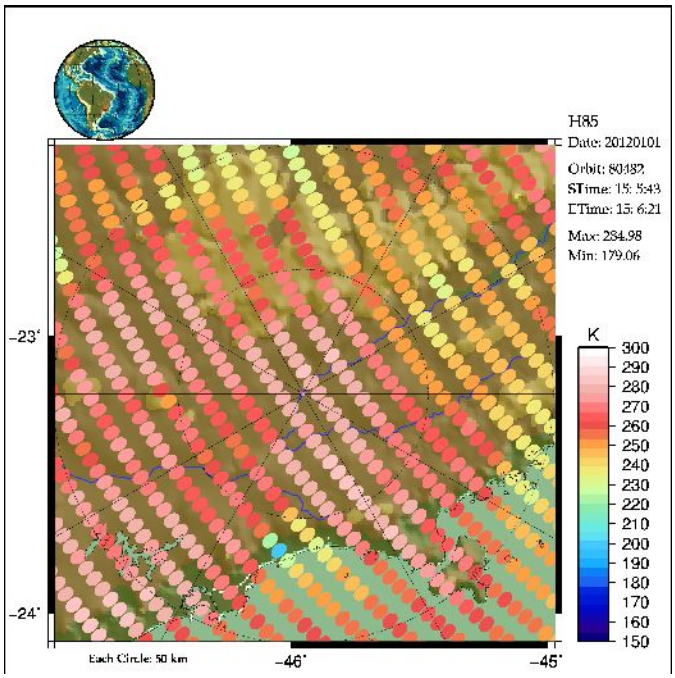

***Figure 6.2**: Brightness temperature at 85 GHz for the same day and the same hour as **Figure 6.1**. The pixel size and orientation is at scale.*

Unfortunately, this particular case is not a very actively convective case. On **Figure 6.2** one can see the brightness temperature at 85 GHz-Horizontal associated to the radar image. The picture shows weakly scattering signals South, North and East of the radar and an even weaker scattering signal in the West.

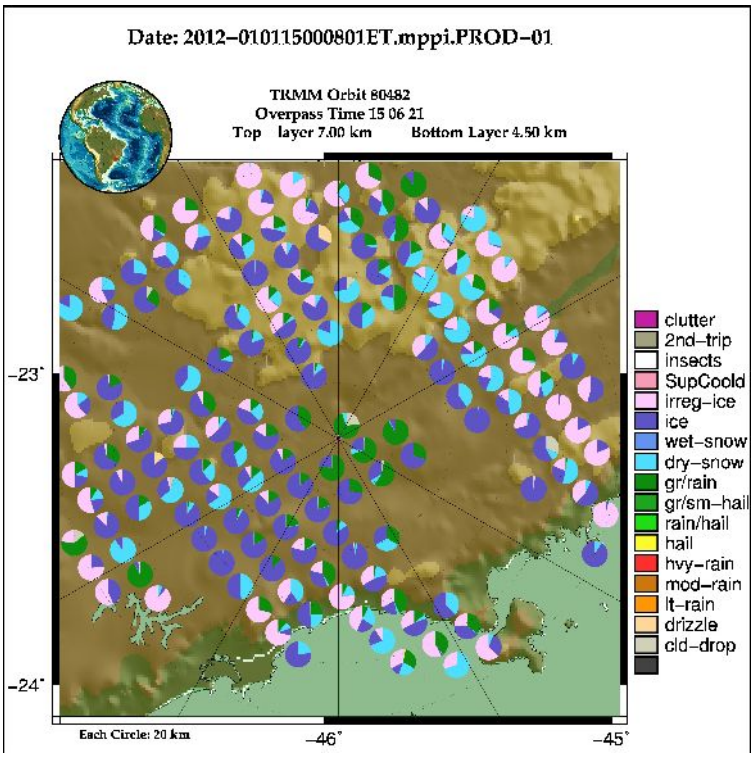

***Figure 6.3**: PID found in each pixel of the TMI overpass on January 1st 2012 at 15:00 UTC over the X-band radar in*

Vale do Paraiba. Each circle is colored proportionally to the number of radar bin of a given species between 7 and 4.5 km altitude within the TMI pixel. Only every other TMI pixel is plotted for the sake of clarity.

Figure 6.3 shows the pie wedge associated with the TMI pixels. For clarity only every other TMI pixel was considered. Each pie wedge represents the proportion of each type of particles found within the pixel radius and within a layer between 4.5 and 7 km where the maximum sensitivity of the 85 GHz channel is expected to be.

The 85 GHz signal will be a combination of both the particle type and the total amount of ice in the column. On the one hand, the denser and/or the larger the particles, the more efficient their scattering. On the other hand, the smaller particles are usually denser than the larger ones. The ice content is easier because it will act directly in proportion of its value: the more ice, the more scattering. These various effects will combine to affect the brightness temperature.

Unfortunately, very little quantitative information is given about the so called species in Keenan (2003) paper. Wet Snow and wet graupel are basically particles found in or near the melting layer, while their dry counterparts are usually found aloft. We can assume that the snow vs. graupel refers to light particles for the former with densities around 0.1 g.cm^{-3} while the latter probably refers to medium-density types with densities around 0.4 g.cm^{-3}. These numbers are pretty standard and used in most model parameterization, either cloud models or radiative transfer models with three or four ice species.

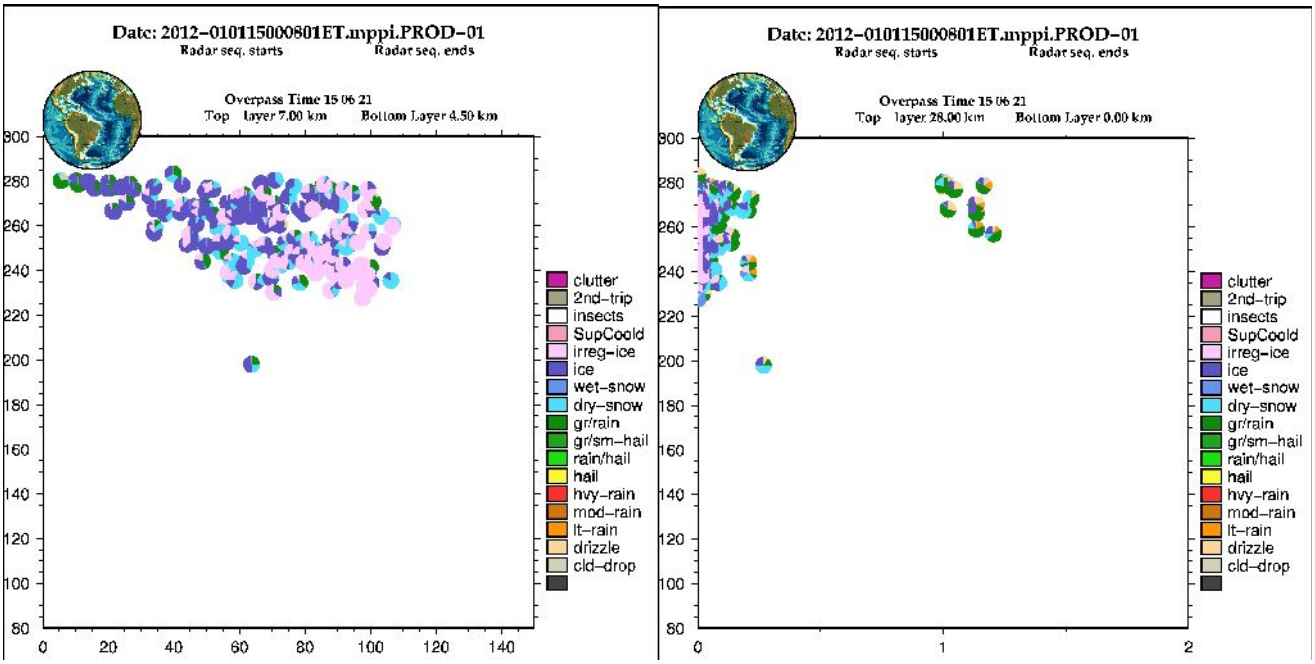

***Figure 6.4**: dependence of the 85 GHz brightness temperature as a function of distance to the radar in km (left) and integrated ice content in kg.m^{-2} (right). Be aware that the considered layers are different in the two graphs.*

Figure 6.4 shows the same piewedge diagram distributed as a function of the 85 GHz brightness temperature along the y-axis and the distance to the radar and the integrated ice content respectively on the x-axis. The first graph (left) shows that a lot of irregular ice is found at greater distance of the radar while simple ice is found at closer distance. This could eventually be an artifact due to attenuation correction and would need to be consolidated on other cases as some of the classes can be very dependent on the reflectivity itself. The second graph (right) shows the more physical results where the integrated ice content and the brightness temperature should be strongly correlated

if not tempered by the particles type. Indeed, high contents of lighter particles (snow) can lead to the same scattering signature (hence the same brightness temperature) as fewer denser particles (e. g. graupels). In the left hand side of **Figure 6.4** such result is not obvious. The few pixels with a substantial number of graupel-like particles are those with the largest ice content but they are not necessarily the coldest pixels associated to the convective cell where the maximum reflectivity is detected on **Figure 6.0**. These large amount of graupels seem a little excessive in regard of the brightness temperature minimum observed on **Figure 6.2** where the scattering signatures are rather weak. This will need to be investigated in more details and will be presented at the CHUVA international conference in May 2012 in Sao Paulo.

7. Teaching activities, seminar and conferences presentation

On the course of my visit, I gave a seminar at INPE/CPTEC in Cachoeira Paulista on the scientific activities related to Megha-Tropiques in September (see poster below).

In December, I participated for 10 days to the CHUVA-SUL campaign in Santa Maria. I gave there 8 hours of class for undergraduate and graduate students on passive and active microwave remote sensing of rain and the associated retrieval techniques (see presence sheets below).

In December also, I gave in INPE Cachoeira and INPE Sao José dos Campos 9 hours of class for graduate students on the same topic as the Santa Maria series of classes.

The on-going work about PID classification and satellite comparison using CHUVA and DYNAMO data was presented at the *6th IPWG* meeting in Sao José dos Campos in October (extended abstract submitted) and also at the Indo-French Megha-Tropiques meeting in Bangalore in December.

In November, the PID classification and satellite comparison using CHUVA and DYNAMO data was presented at the *5th International TRMM and GPM Conference* in Tokyo Japan.

Both the results on BRAIN and the PID results will be presented at the CHUVA international conference in May 2013 in Sao Paulo and the BRAIN results will be presented at the 2013 EUMETSAT conference in Vienna.

8 Conclusions and perspectives

With the aim of improving the detection of warm rain situation over Brasil, a new version of BRAIN was developed which is supposed to better use the available information from the brightness temperatures and also give a more complete answer than the usual Bayesian schemes (e. g. Gprof algorithm, or previous versions of BRAIN). Namely, these algorithm simply retrieve rain as an weighted average of a number of neighboring elements in an a-priori database. But the Bayesian scheme contains more information than just the average (expectation) rain rate as a solution since it can tell us also the probability associated with the various individuals of the retrieval (a-priori) database. These ideas are fairly new and have not been exploited in the rain retrieval community to our knowledge. A large part of the visit was dedicated to developing these new paradigm for rain retrieval and we do believe that there is a great potential here. Nonetheless, the new version of BRAIN requires some polishing before it is brought to its optimal performances. The errors are still larger than they should be, particularly over land which is always more difficult to adjust.

We have, for that purpose, developed a new and enlarged retrieval database that will be used in the future not only for TMI but also for SSMI, SSMIS, MADRAS and AMSR-2, making the BRAIN series a complete set of instantaneous rain retrieval that will be used by DSA-CPTEC in collaboration with Daniel Vila in particular. The developed version when fully operational will offer cutting-edge new results in terms of probabilistic retrievals. This results will be published in 2013 as soon as the BRAIN version is finalized. In the meantime, these new concept will be presented at the CHUVA international conference in May, the EUMETSAT conference in April and the PMM meeting in March.

We have not developed a South-America-dedicated database as we feel that this might not be the best way to carry on improving retrievals. This position could be revised in the future and some tests will need to be performed in the forthcoming month. The problem with regional database is the difficulty to build a good representativeness of the regional events, without loosing the capability to capture “unusual” situations. These questions are actually extremely up-to-date in the rain retrieval community and are not, to this day, answered on a definite manner.

We have tried to combine ForTraCC life cycle information to BRAIN retrieval. This task has appeared more difficult than anticipated. The general principle of the combination is rather simple and the physics beyond it is well understood, but the practical aspect of it is made very hard by the difficulty to define the life cycle of systems. This concept of beginning-middle-end of life for convection is robust on a statistical sense but very noisy when looking at individual systems because convection follows complex patterns involving merging, splitting, large and small scales altogether etc... Some encouraging results have shown that the microphysics and the life cycle could be well correlated on a statistical basis and further developments will be pursued in 2013 in particular over regions (Amazon) where convection might be more easily defined as a “pure” meso-scale feature rather than a synoptic-scale driven event. The results on microphysics and brightness temperature evolution as a function of the life cycle will be the object of a publication in 2013 if the results are consolidated.

The comparisons between the X-band radar, the associated PID and the satellite brightness temperature will be continued with the help of Dra. Pra. A. Martini at LATMOS, strengthening the collaborative effort between DSA and the latter. These results are the first one of their nature and specially the use of pie-wedge representation to exploit non-continuous variable (particles species) and build statistics. These results will hopefully be the object of a publication in 2013 and will be presented at the CHUVA international conference. They were already presented at the 6th IPWG conference and the 2nd French-Indian Megha-Tropiques Scientific Conference. Furthermore, more systematic comparisons between the CHUVA radar and the BRAIN retrieval from the various instruments (TMI, SSMI, SSMIS, AMSR-2) will be conduced in the near future to better assess the performances of the new algorithm and relate these performances to the local and regional condition of the convection. The latter topic is obviously a longer term goal.

On the overall, I do believe that this visit, although it did not give as many results as expected in particular on the “life cycle” aspect and the “warm rain” aspect, will have numerous outcomes. It will certainly add some values to the CHUVA data by strengthening the connection with Megha-Tropiques and the GPM community, and in turn these data are a valuable addition to the validation efforts funded by CNES in this same context.

There is little doubt that following this visit we will have some leverage to request doc and post-doc funding from the French agencies for Brasilian students and researchers on the same topics to pursue the efforts.

ANNEXES

Dr. Nicolas Viltard

Laboratoire Atmosphères, Milieux, Observations Spatiales (LATMOS0 - France)

Wednesday September 5 2:00 PM - CPTEC/INPE

Rodovia Presidente Dutra, km 39 – Cachoeira Paulista - SP

He is strongly involved in the French-Indian cooperation on the Megha-Tropiques mission to study the water and energy cycle in the Tropics. This satellite was launched in October 2011 on a low inclination orbit (20°), allowing for the first time an exceptional sampling of the 30N-30S region. The three instruments on board are meant to measure the water vapor profile (SAPHIR), the radiative budget at the top of the atmosphere (ScaraB) and the precipitation (MADRAS). All three instruments are passive radiometers, ScaraB sampling the visible-infrared domain while SAPHIR and MADRAS are microwave instruments.

The presentation will give a brief overview of the Megha-Tropiques satellite and of the research activities associated. A particular emphasis will be made on rain retrieval from the MADRAS (and other radiometers) data using a Bayes-monte-Carlo approach known as BRAIN.

Nicolas Viltard defended his PhD in 1995 at Centre d'étude des Environnements Terrestres et Planétaires (CETP) in Paris on dynamics and thermodynamics of tropical cyclones using airborne radar data. He then started to work on rain retrieval from satellite data using SSMI from DMSP over the TOGA-COARE area. In 1997 and 1998 he spent some time in the TRMM team at Nasa's Goddard Space Flight Center, working on combining the Precipitation Radar (PR) and the TRMM Microwave Imager (TMI) to improve rain retrieval in the tropics. In 1999, he became a researcher for CNRS at LATMOS, in charge of the MADRAS instrument and the rain retrieval on the French-Indian Megha-Tropiques mission. He developed an algorithm known as BRAIN (Bayesian Rain Including Neural network), which is implemented as the operational rain product for Megha-Tropiques. In 2010, he was with Luiz Augusto Toledo Machado the PI of phase 0 of the French-Brazilian project BOITATA.

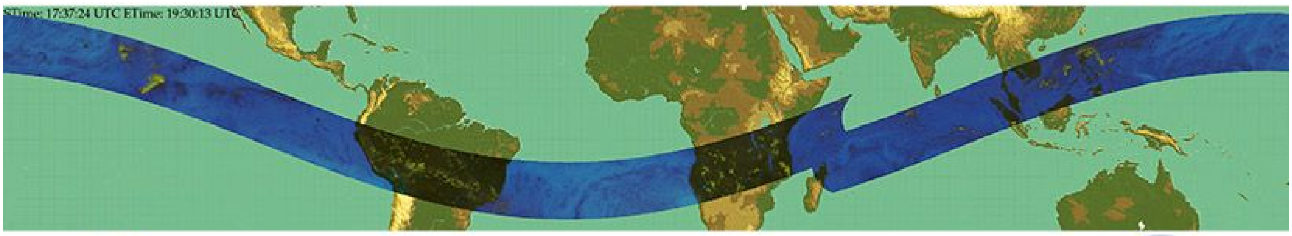

MINISTÉRIO DA CIÊNCIA E TECNOLOGIA
INSTITUTO NACIONAL DE PESQUISAS ESPACIAIS

Difusão do Conhecimento
difusao.conhecimento@cptec.inpe.br

THE SATELLITE MEGHA-TROPIQUES AND THE ASSOCIATED RAIN RETRIEVAL ACTIVITIES

Dr. Nicolas Viltard
Laboratoire Atmosphères, Milieux, Observations Spatiales (LATMOSO – France

Wednesday September 5 2:00 PM

He is strongly involved in the French-Indian cooperation on the Megha-Tropiques mission to study the water and energy cycle in the Tropics. This satellite was launched in October 2011 on a low inclination orbit (20°), allowing for the first time an exceptional sampling of the 30N 30S region. The three instruments on board are meant to measure the water vapor profile (SAPHIR), the radiative budget at the top of the atmosphere (ScaraB) and the precipitation (MADRAS). All three instruments are passive radiometers, ScaraB sampling the visible-infrared domain while SAPHIR and MADRAS are microwave instruments.

The presentation will give a brief overview of the Megha-Tropiques satellite and of the research activities associated. A particular emphasis will be made on rain retrieval from the MADRAS (and other radiometers) data using a Bayes-monte-Carlo approach known as BRAIN.

1) Joyhy Sakevas
2) Alan Pathias
3) Ingrid Diniz
4) Aline Schneider Fauck
5) Enrique Vieira Mattos
6) Renata Galante Negri
7) Wilber A. Gonçalves
8) Isabelly Carvalho de Castro
9. JURANDIR VARGAS RODRIGUES
10- Roman Campos Braga
11 - WAGNER FLAUBER A LIMA - DSA
12- Eder P. Vendrosco - DSA
13 - ANTHONY GARCIA SILVA CONFINO - DSA/CPTEC/INPE
14 - Thomas Fiolleau
15 - Thiago S. Biscaro
16 - RACHEL ALBRECHT
17 Rosika P. Rodrigues CPTEC/INPE
18 - Sergio Henrique S. Ferreira CPTEC/INPE
19 - RAYANA SANTOS ARAÚJO CPTEC/INPE
20. Simone Sievert CPTEC/INPE
21. Juan Carlos Ceballos